Full Title: **Cyfip2 controls the acoustic startle threshold through FMRP, actin polymerization, and $GABA_B$ receptor function.**

Short Title: **Cyfip2 controls startle sensitivity via FMRP, Rac1 and $GABA_B$ receptors.**

Jacob C. Deslauriers[1], Rohit P. Ghotkar[1,3], Lindsey A. Russ[1,4], Jordan A. Jarman[1,5], Rubia A. Martin[1,6], Rachel G. Tippett[1], Sureni H. Sumathipala[1], Derek F. Burton[1,7], D. Chris Cole[1], Kurt C. Marsden*[1,2]

1. Department of Biological Sciences, North Carolina State University, Raleigh, North Carolina, USA
2. Center for Human Health and the Environment (CHHE), North Carolina State University, Raleigh, North Carolina, USA
3. Current address: Putnam Associates, Boston, Massachusetts, USA
4. Current address: Department of Pharmacology & Physiology, Georgetown University, Washington D.C., USA
5. Current address: Department of Physiology and Biophysics, Boston University, Boston, MA, USA
6. Current address: U.S. Environmental Protection Agency, Raleigh-Durham-Chapel Hill, North Carolina, USA
7. Current address: Biogen, Durham, North Carolina, USA

*Corresponding author: kcmarsde@ncsu.edu

Author contributions: Conceptualization: JCD and KCM; Data curation: JCD, RAM; Formal analysis: JCD, RAM, RGT, SHS, DCC, KCM; Funding acquisition: KCM; Investigation: JCD, RPG, LAR, JAJ, RAM, RGT, SHS, DFB, DCC, KCM; Methodology: JCD, RAM, KCM; Project administration: KCM; Supervision: JCD, DFB, DCC, KCM; Visualization: JCD, RAM, KCM; Writing – original draft: JCD; Writing – review and editing: JCD, KCM

Abstract

Animals process a constant stream of sensory input, and to survive they must detect and respond to dangerous stimuli while ignoring innocuous or irrelevant ones. Behavioral responses are elicited when certain properties of a stimulus such as its intensity or size reach a critical value, and such behavioral thresholds can be a simple and effective mechanism to filter sensory information and determine if a response is appropriate. For example, the acoustic startle response is a conserved and stereotyped defensive behavior induced by sudden loud sounds, but dysregulation of the threshold to initiate this behavior can result in startle hypersensitivity that is associated with sensory processing disorders including schizophrenia and autism. Through a previous forward genetic screen for regulators of the startle threshold a nonsense mutation in *Cytoplasmic Fragile X Messenger Ribonucleoprotein (FMRP)-interacting protein 2* (*cyfip2*) was found that causes startle hypersensitivity in zebrafish larvae, but the molecular mechanisms by which Cyfip2 establishes the acoustic startle threshold are unknown. Here we use conditional transgenic rescue and CRISPR/Cas9 gene knockdown approaches to determine that Cyfip2 requires both Rac1 and FMRP pathways, but not the closely related FXR1 or FXR2, to regulate the acoustic startle threshold in early neurodevelopment. Using a candidate-based drug screen we find that Cyfip2 also acts acutely to maintain the startle threshold through Arp2/3-mediated branched actin polymerization and N-methyl D-aspartate receptors (NMDARs). To identify proteins and pathways that may be targets of Cyfip2-FMRP-mediated translational regulation, we then performed discovery proteomics and determined that loss of Cyfip2 alters cytoskeletal and extracellular matrix components and disrupts oxidative phosphorylation and GABA receptor signaling. Finally, we validated our proteomics findings by showing that the $GABA_B$ receptor agonist baclofen, but not the $GABA_A$ agonist muscimol, restores normal startle sensitivity in *cyfip2* mutants. Together, these data reveal that Cyfip2 acts through multiple pathways to regulate excitatory/inhibitory balance in the startle circuit to control the processing of acoustic information.

Introduction

To navigate their environments to find food and avoid predation, animals must be able to filter out extraneous stimuli but respond appropriately to salient ones, a process known as sensorimotor gating. Specific attributes of a stimulus can trigger a response; for visual stimuli the luminance, size, and speed of the stimulus determine if escape and reorientation responses are initiated [1–3]. Similarly, the intensity and frequency of acoustic stimuli determine whether a response is made [4,5]. One way in which animals can control their responses to sensory stimuli is by establishing a behavioral threshold such that when one or more of these stimulus attributes reaches a critical value a specific behavioral response is initiated. Behavioral thresholds are a fundamental mechanism of sensorimotor gating used across the animal kingdom to regulate a wide range of behavioral responses including both collective responses, such as fanning behaviors for hive climate regulation in bees [6,7] and shoaling behavior in fish [8,9], as well as individual responses to odors [10–13], tactile stimuli [14–17], changes in luminance and contrast of visual stimuli [1,18–21], and sound frequency and intensity in mammals and fish [5,22–24]. That behavioral over-responsiveness to visual, tactile, and acoustic stimuli is observed across a number of neuropsychiatric conditions including autism, anxiety, and schizophrenia [4,22,24–28] highlights the importance of setting such behavioral thresholds at an appropriate level. Yet our knowledge of the molecular mechanisms that both establish and maintain behavioral thresholds is limited.

Previously, to identify genes that regulate the threshold for initiating the acoustic startle response, a highly conserved behavior initiated following sudden loud sounds that may indicate danger [5,29–31], we conducted a standard 3-generation, ENU-based forward genetic screen in larval zebrafish [32]. We identified a set of five mutant lines that display acoustic startle hypersensitivity, and through whole-genome sequencing of the *triggerhappy* mutant line, we identified a causal, nonsense mutation in *cytoplasmic Fragile X Messenger Ribonucleoprotein (FMRP)-Interacting protein 2* (*cyfip2).* Cyfip2 was first identified as an interactor of FMRP and

the elongation initiation factor 4E (eIF4E), through which it participates in translational repression of many target transcripts [33,34]. Cyfip2, but not the closely related Cyfip1, can also bind the Fragile X-related proteins FXR1 and FXR2, but the function of these interactions is unknown [33]. Additionally, Cyfip2 interacts with the activated form of the small Rho GTPase Rac1, and it is a member of the WAVE Regulatory Complex (WRC) in which it helps regulate Arp2/3 activation and branched actin polymerization [35–41]. Cyfip2 is vital for proper neuronal migration and cell movement, axonal growth and guidance, as well as synapse formation and function in flies, mice, and zebrafish [32,33,37,42–47]. Homozygous *cyfip2* mutations are embryonically lethal in mammals and fatal after 7-8 days post-fertilization (dpf) in zebrafish [32,42,44,48]. Despite its key role in multiple aspects of neurodevelopment, the links between how Cyfip2 regulates RNA translation, actin polymerization, and behavior have not been defined. Our previous work demonstrated that loss of Cyfip2 causes acoustic startle hypersensitivity that is reversible upon transgenic expression of GFP-tagged Cyfip2, alters the morphology but not the electrophysiological properties of the startle command-like Mauthner cells (M-cells), and causes hyperexcitability of the spiral fiber neurons (SFNs), a set of hindbrain excitatory interneurons that project to the M-cell axon hillock [32]. It is unclear, however, whether Cyfip2 acts via Rac1-mediated actin polymerization or through FMRP-mediated translational repression to control the startle threshold. Furthermore, the downstream molecular changes that directly modulate the function of the startle circuit have not been identified.

In this study we used an inducible rescue approach in *cyfip2* mutant zebrafish larvae to demonstrate that both Cyfip2's Rac1 and FMRP interactions are required for establishing the acoustic startle threshold during early neurodevelopment. Using CRISPR-Cas9 gene knockdown we find that FXR1 and FXR2 are dispensable for startle regulation and that Cyfip2 acts through FMRP. Furthermore, with a candidate-based pharmacological approach we show that Cyfip2 mediates Arp2/3-induced branched actin polymerization and may modulate N-methyl-D-aspartate receptors (NMDARs) to alter neuronal function in the acoustic startle circuit.

Finally, we performed discovery proteomics to define molecular pathways disrupted by loss of Cyfip2 *in vivo*. Our results indicate roles for Cyfip2 in mitochondrial function, oxidative phosphorylation, and inhibitory Gamma-Aminobutyric Acid (GABA) receptor signaling. We confirmed the functional importance of this last finding using the $GABA_B$ receptor agonist baclofen, which rescues *cyfip2* mutants' hypersensitivity. Together these data establish a novel pathway that links Cyfip2, actin dynamics, RNA translation, and excitatory/inhibitory balance in the control of acoustic responsiveness.

Results

Cyfip2 establishes the acoustic startle threshold through both Rac1 and FMRP.

Cyfip2 has four known protein-interaction domains [49] (Fig. 1A), and it can act through Rac1 to promote actin polymerization (Fig. 1B) and FMRP to regulate RNA translation (Fig. 1C). *cyfip2*^{p400} mutants have a single base pair transversion (nt1024; T to A) resulting in a premature stop codon at amino acid position 343 (Fig. 1A) [32]. *cyfip2*^{p400} mutant zebrafish larvae (5 dpf) were previously shown to display acoustic startle hypersensitivity that could be rescued by expressing Cyfip2 at 30 hours post fertilization (hpf) using a stable heatshock-inducible transgenic line, *Tg(hsp70:cyfip2-EGFP)* [32]. We replicate those findings here, using a 60-stimulus assay consisting of 10 trials at each of 6 intensities with a 20 second (s) interstimulus interval (ISI) to measure startle sensitivity (Fig. 1D). A 40-min heatshock at 30 hpf restores normal sensitivity in transgenic (*Tg*+) but not in non-transgenic (*Tg*-) *cyfip2* mutants (Fig. 1D,E). Previous studies have established that C179R and K723E amino acid substitutions prevent Cyfip2 from binding with Rac1 and FMRP, respectively [34,39,45]. To determine if Cyfip2 engages Rac1-mediated actin regulation and/or FMRP/eIF4E-mediated translational repression pathways to establish the acoustic startle threshold, we induced C179R (Δ*Rac1*) and K723E (Δ*FMRP*) point mutations in the *Tg(hsp70:cyfip2-EGFP)* construct and created stable transgenic lines for each (Fig. 1A). We expressed either wildtype or mutant (Δ*Rac1*; Δ*FMRP)* versions of

Cyfip2 in mutants at 30 hpf with a 40-minute heatshock at 38°C, followed by acoustic startle testing at 5 dpf. While expression of wildtype *Tg(hsp70:cyfip2-EGFP)* at 30 hpf rescues mutant hypersensitivity, expression of Δ*Rac1* or Δ*FMRP* versions of Cyfip2 in mutants was insufficient to rescue mutant hypersensitivity (Fig. 1E).

cyfip2 mutants also display a number of kinematic defects in their performance of the startle response [32]. To determine if Rac1 and FMRP binding are also required for Cyfip2 to regulate startle kinematics, we analyzed startle latency, duration, head turn angle (C1 angle), and total distance traveled during the response in *Tg*- and *Tg*+ fish after the same 40-min heatshock protocol at 30 hpf (Fig. S1). Heatshock induction of wildtype Cyfip2 restored normal latency, duration, and C1 angle, but not distance traveled (Fig. S1). All kinematic defects remained in *cyfip2* mutant larvae expressing Δ*Rac1*-Cyfip2 (Fig. S1), but expression of Δ*FMRP*-Cyfip2 was sufficient to rescue startle duration and induced a trend toward rescue of startle latency and C1 turn angle (Fig. S1). These data suggest that Rac1 binding is required for all aspects of Cyfip2-mediated startle regulation, while FMRP binding is required to regulate the startle threshold but is largely dispensable for startle kinematics.

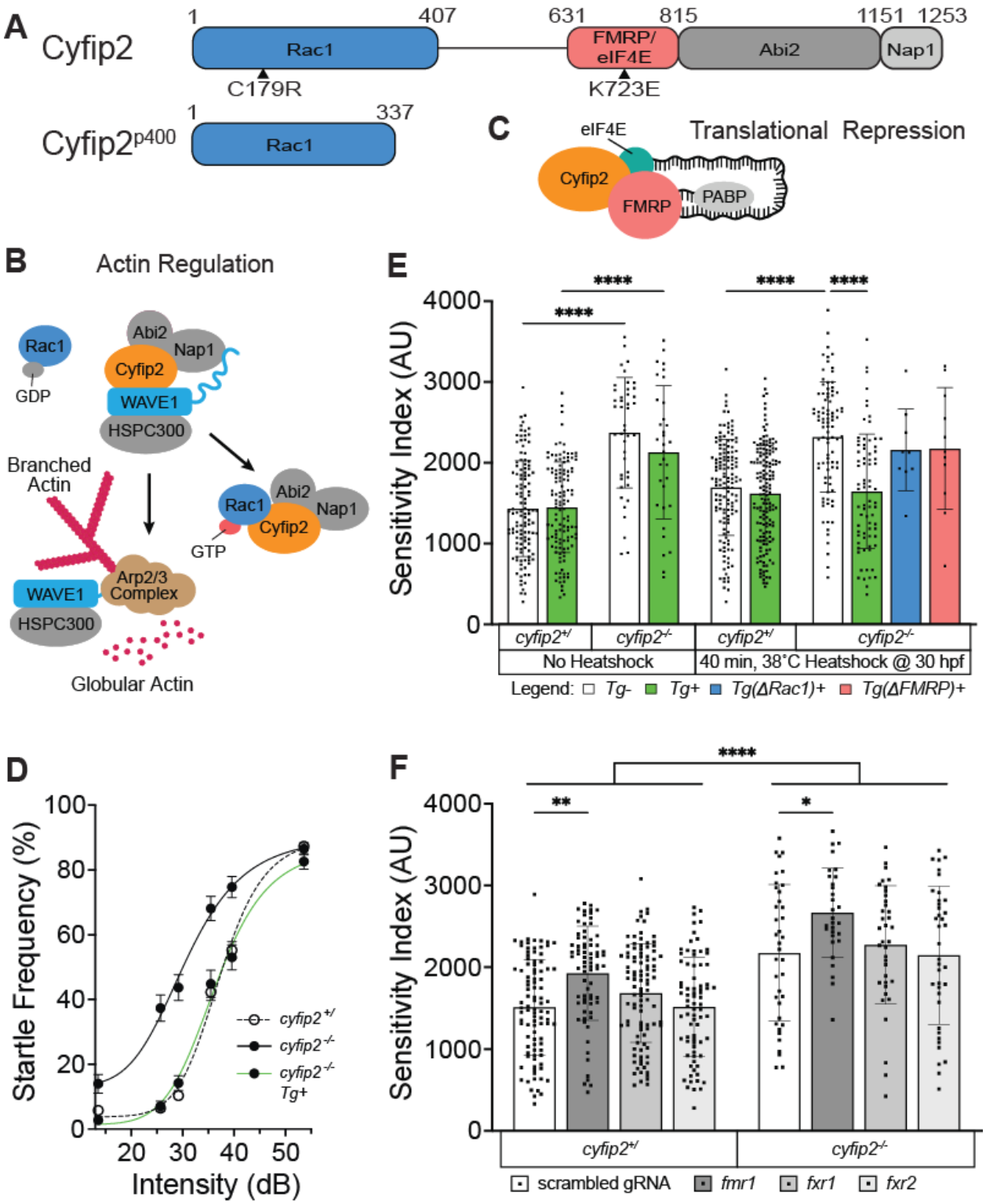

Figure 1. Cyfip2 establishes the acoustic startle threshold through Rac1 and FMRP. (A) Cyfip2 protein interacting domain diagram of wildtype (top) and mutant (bottom) Cyfip2 proteins. Black arrowheads indicate the positions of induced mutations in Cyfip2, eliminating the Rac1- (C179R) or FMRP/eIF4E (K723E)-binding capacity of Cyfip2. (B) Cyfip2 actin regulatory pathway wherein Cyfip2 (orange) upon stimulation by Rac1-GTP triggers WAVE1 activation, Arp2/3-complex initiation and branched actin nucleation. (C) Cyfip2 translational repression pathway in which Cyfip2, eIF4E (teal), and

FMRP (pink) along with the poly-A binding protein (PABP; gray), sequester neurodevelopmentally important mRNAs from being translated. (D) Average startle frequency (%) after 10 trials at 13.6, 25.7, 29.2, 35.5, 39.6 and 53.6 dB for 5 dpf *cyfip2* siblings (+/) and mutant (-/-) larvae heatshocked at 30 hpf for 40 minutes at 38˚C. The average startle frequency curve for *cyfip2* siblings (+/; open circles, dashed line), *cyfip2* mutants (-/-; closed circles, solid line) and *cyfip2* mutants harboring the *Tg(hsp70:cyfip2-EGFP)*+ transgene (-/-; Tg+; closed circles, solid green line). (E) Sensitivity indices, calculated as the area under the startle frequency curves, for 5 dpf *cyfip2* siblings and mutants, following a 40-minute heatshock at 30 hpf to express either wildtype (*Tg*+; green), Rac1- (Δ*Rac1*+; blue) or FMRP/eIF4E- (Δ*FMRP*+; pink) binding deficient versions of Cyfip2-EGFP. Comparisons were made to both non-transgenic (*Tg*-) and non-heatshocked controls. All indices (mean ± SD) compared using a Kruskal-Wallis test with Dunn's multiple comparisons correction; p**** < 0.0001. (F) Sensitivity indices for 5 dpf *cyfip2* sibling (+/) and mutant (-/-) larvae following 1-cell stage injection with CRISPR-Cas9 and a single, *scrambled* guide RNA (gRNA) or dual gRNA cocktails targeting *fmr1*, *fxr1,* or *fxr2*. *scrambled* gRNA injected (white bar, closed circles); *fmr1* gRNA injected (dark gray bar closed circles); *fxr1* gRNA injected (medium gray bar; closed circles); *fxr2* gRNA injected (light gray bar, closed circles). Comparisons were made both within genotype and between genotypes by condition. All indices (mean ± SD) compared using an Ordinary one-way ANOVA with Sidak's multiple comparisons correction; p* < 0.05; p** < 0.01; p**** < 0.0001.

One possible explanation for these results is that expression levels may differ between the three heatshock transgenic lines. We therefore measured expression levels of each transgenic Cyfip2-GFP protein 6 hours after a 40-min heatshock by fluorescence intensity (Fig. S2A). The Δ*Rac1* and Δ*FMRP* lines displayed GFP expression that was not significantly different than the wildtype *Tg*+ line but which trended lower. To induce expression of wildtype Cyfip2-GFP at levels more comparable to the Δ*Rac1* and Δ*FMRP* lines after 40-minute heatshock, we delivered a 15-min heatshock at 30 hpf in the wildtype *Tg*+ line. The 15-min heatshock reduced peak Cyfip2-GFP expression to levels comparable to or below that of the Δ*Rac1* and Δ*FMRP* lines, and this level of expression was also sufficient to rescue acoustic startle sensitivity in *cyfip2* mutants (Fig. S2A-C). Thus, the level of transgene expression cannot account for the failure of the Δ*Rac1* and Δ*FMRP* constructs to rescue startle phenotypes, and these findings support our conclusion that Cyfip2 utilizes both Rac1- and FMRP-mediated pathways to establish the acoustic startle threshold.

<u>Cyfip2 acts through FMRP but not FXR1/2 to establish the acoustic startle threshold.</u>

We previously found that FMRP is not required to establish a normal startle threshold, as *fmr1*^{hu2787} mutants' startle sensitivity is unaffected [32]. Having established that the K723 residue

that Cyfip2 uses to bind FMRP is required for normal startle sensitivity, however, we hypothesized that Cyfip2 may instead interact with other members of the Fragile X protein family, Fragile X-related proteins 1 and 2 (FXR1/2), to establish the acoustic startle threshold [33]. We designed pairs of CRISPR guide RNAs (gRNAs) targeting each of the *fmr1, fxr1* and *fxr2* genes. We injected *fmr1*-, *fxr1*- or *fxr2*-specific CRISPR-Cas9 cocktails into 1-cell stage *cyfip2* sibling and mutant embryos and measured acoustic startle sensitivity in these crispant larvae at 5 dpf (Fig. 1F). Highly efficient CRISPR-induced mutagenesis was observed for all 3 genes, with 4 of the 6 gRNAs inducing edits as confirmed by PCR amplification and Sanger sequencing (Fig. S3A-F). Quantitative PCR confirmed that mRNA expression of all three genes was strongly reduced by CRISPR/Cas9 injection (Fig. S3G). FMRP crispants had significantly increased startle sensitivity compared to larvae injected with a scrambled gRNA plus Cas9, and sensitivity of FMRP crispants was even further increased in the *cyfip2* mutant background (Fig. 1F). However, startle sensitivity was unaltered in FXR1 or FXR2 crispants in either *cyfip2* siblings or mutants (Fig. 1F). These data indicate that FMRP, but not FXR1/2, regulates the startle threshold. The discrepancy between our hypersensitive FMRP crispants and prior analysis of non-hypersensitive mutants from the ENU-induced *fmr1*^{hu2787} line is likely due to the different methods used to generate these lines. Indeed, a recent study has shown that there is substantial genomic adaptation in the *fmr1*^{hu2787} mutant line that may partially compensate for the loss of FMRP [50], and an independently created CRISPR-induced *fmr1* mutant line displayed additional behavioral and developmental phenotypes not seen in the *fmr1*^{hu2787} line [51]. Thus, together with these findings our data indicate that Cyfip2 acts in part through FMRP to establish the startle threshold.

<u>Cyfip2 maintains the acoustic startle threshold through Rac1 and FMRP pathways throughout early neurodevelopment.</u>

Our previous study found that Cyfip2 is important for both establishing the acoustic startle threshold during early neurodevelopment, and for actively modulating the threshold later in development between 4 and 6 dpf [32]. Here we sought to define a critical window for Cyfip2 expression in regulating the startle threshold using our heatshock transgenic lines. Our results show that while a 40-minute heatshock to induce expression of wildtype Cyfip2 (*Tg*+) at 30 hpf is sufficient for behavioral rescue in 5 dpf *cyfip2* mutant larvae (Fig. 1D,E), a 40-min heatshock at 2, 3, or 4 dpf fails to rescue *cyfip2* mutant hypersensitivity (Fig. S4). Heatshock-induced expression at 5 dpf, 4 hours prior to testing, resulted in a trend toward rescue and a bi-modal distribution with some *cyfip2* mutants remaining hypersensitive and a second population showing restoration of normal sensitivity (Fig. 2A). These results are similar to our prior findings [32], and they suggest that Cyfip2 can not only function in the development of the startle circuit but can also actively maintain the circuit's threshold after it has formed. Next, to determine if Cyfip2 employs both of its canonical pathways in maintaining the startle threshold after 4 dpf, we expressed either Δ*Rac1* or Δ*FMRP* versions of Cyfip2 in *cyfip2* mutants at 5 dpf with a 40-min heatshock followed by acoustic startle behavior testing 6 hours later. Similar to what we observed with the developmental heatshock (Fig. 1E), neither expression of Δ*Rac1* nor ΔFMRP Cyfip2 at 5 dpf rescued acoustic hypersensitivity in mutants (Fig 2A). These findings suggest that Cyfip2 uses both its Rac1- and FMRP-mediated pathways to both establish and dynamically maintain the acoustic startle threshold throughout neurodevelopment.

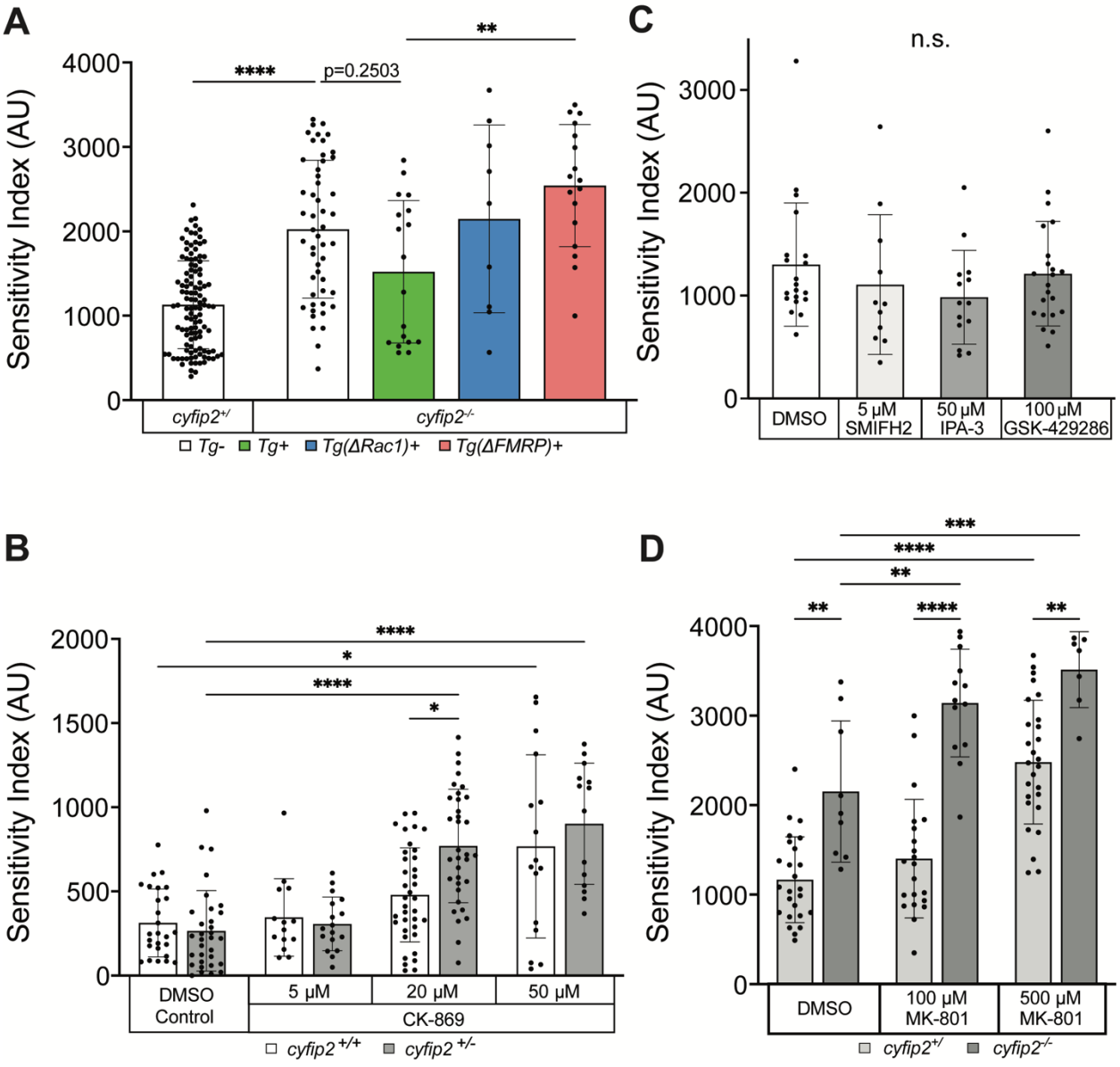

Figure 2. Cyfip2 acutely regulates branched actin polymerization and NMDARs to establish the acoustic startle threshold. (A) Sensitivity indices for 5 dpf *cyfip2* sibling (+/) and mutant (-/-) larvae, following a 40-minute heatshock at 120 hpf (5 dpf) to express either wildtype (*Tg*+; green), Rac1- (Δ*Rac1*+; blue) or FMRP/eIF4E- (Δ*FMRP*+; pink) binding deficient versions of Cyfip2-EGFP. Comparisons were made to non-transgenic (*Tg*-), heatshocked sibling (+/) and mutant (-/-) controls. All indices (mean ± SD) compared using a Kruskal-Wallis test with Dunn's multiple comparisons correction; p-values listed; p** < 0.01, p**** < 0.0001. (B) Sensitivity indices for 5 dpf *cyfip2* wildtype (+/+; white bar) and heterozygous (+/-; gray bar) larvae, treated for 30 minutes on d5 with 5, 20 or 50 μM CK-869. Comparisons were made both within genotype and within condition. All indices (mean ± SD) compared using a Kruskal-Wallis test with Dunn's multiple comparisons correction; p* < 0.05; p**** < 0.0001. (C) Sensitivity indices for 5 dpf Tüpfel longfin (TLF) larvae treated for 30 minutes on d5 with the highest, non-lethal doses the formin antagonist (SMIFH2; 5 μM), PAK3 antagonist (IPA-3; 50 μM) and ROCK antagonist (GSK429286; 100 μM). Comparisons were made between respective treatments and the DMSO controls. All indices (mean ± SD) were compared using a Kruskal-Wallis test with Dunn's multiple comparisons correction; All comparisons made were non-significant (n.s.). (D) Sensitivity indices for 5 dpf *cyfip2* sibling (+/) and mutant (-/-) larvae, treated for 30 minutes on d5 with 100 or 500 μM MK-801.

Comparisons were made both between genotypes within condition and between conditions by genotype. All indices (mean ± SD) were compared using an Ordinary one-way ANOVA with Tukey's multiple comparisons correction. p** < 0.01; p*** < 0.001; p**** < 0.0001.

Cyfip2 maintains the acoustic startle threshold through branched actin polymerization.

Regulation of the actin cytoskeleton is a vital cellular process that within the context of the nervous system is critical for cell migration and movement, synapse formation, function and plasticity, receptor anchoring and trafficking, as well as axon growth and guidance [52]. Given our findings that Cyfip2 can act through the Rac1-WAVE pathway to establish and modulate the acoustic startle threshold, we hypothesized that Cyfip2-mediated branched actin polymerization specifically modulates the startle threshold. To test this hypothesis, we incubated 5 dpf *cyfip2* heterozygous and wildtype larvae in the Arp2/3 antagonist CK-869 at 5, 20, or 50 μM for 30 minutes, followed by acoustic startle testing. In control conditions, *cyfip2* heterozygotes display startle sensitivity equal to that of wildtypes (Fig. 2B), and incubation at 5 μM did not significantly alter startle sensitivity of either heterozygotes or wildtypes (Fig 2B). At 20 μM, wildtype larvae are unaffected by CK-869, but *cyfip2* heterozygotes have significantly increased startle sensitivity compared to controls (Fig 2B). 50 μM CK-869 caused both *cyfip2* wildtype and heterozygous larvae to become significantly hypersensitive compared to controls, phenocopying *cyfip2* mutants. Thus, Arp2/3-mediated, branched actin polymerization is necessary for acutely maintaining the acoustic startle threshold. That *cyfip2* heterozygotes display hypersensitivity at 20 μM but wildtypes do not indicates that a single functional copy of *cyfip2* is insufficient to maintain normal startle circuit function when branched actin polymerization is limited by a moderate dose of CK-869. We found similar results when exposing larvae to another Arp2/3 antagonist, CK-666, with both *cyfip2* heterozygotes and wildtypes phenocopying mutant hypersensitivity at a 50 μM concentration (Table S2). These findings support the conclusion that Cyfip2-dependent Arp2/3-mediated branched actin polymerization is necessary to maintain the acoustic startle threshold.

The actin cytoskeleton is dynamic and requires the action of both branched and unbranched actin regulatory pathways to maintain cellular structure and function. Unbranched filamentous (F) actin is polymerized from globular actin monomers by dimeric complexes of formin proteins, which bind at the barbed ends of new filaments and promote their elongation [53–56]. Another form of actin regulation involves the action of cofilin, an actin severing protein that cleaves existing filaments to create new barbed ends and increase the rate of actin turnover within the cell [57]. To determine whether unbranched actin and severing pathways play a role in regulating the acoustic startle threshold we incubated 5 dpf wildtype larvae in a formin antagonist, SMIFH2, or the cofilin disinhibitors, IPA-3 and GSK429286, for 30 minutes followed by acoustic startle testing. Treatment with 5 μM SMIFH2 or with 50 μM IPA-3 or 100 μM GSK429286 did not significantly affect startle sensitivity in wildtype larvae (Fig 2C). We also tested these drugs at higher concentrations, which were lethal after a 30-minute exposure, as well as longer exposures at lower concentrations, which had no effect on startle sensitivity (Table S1). Our data with the formin inhibitor SMIFH2 are in contrast to a recent finding showing that Formin 2B morpholino knockdown caused a decrease in Mauthner cell-mediated fast startle responses in zebrafish larvae [58]. That we did not observe any change in startle frequency is likely due to the acute nature of our pharmacological approach as opposed to the morpholino-mediated developmental knockdown of Formin 2B. Our findings suggest that acute perturbations to unbranched actin filaments and actin turnover do not play a significant role in regulating the acoustic startle threshold. Altogether these data further support our conclusion that Cyfip2-mediated, branched actin polymerization is a key pathway for acutely maintaining the acoustic startle threshold.

<u>Cyfip2 may regulate NMDA receptors to modulate the acoustic startle threshold.</u>

While we have established that Cyfip2 mediates the establishment and maintenance of the acoustic startle threshold through both branched actin and FMRP regulatory pathways, it is

unclear what molecular mechanisms directly modulate the excitability of the startle circuit. To identify molecules that may be downstream effectors of Cyfip2 in modulating activity of the startle circuit, we conducted a candidate-based small-molecule screen with compounds previously shown to alter startle sensitivity in wildtype zebrafish larvae (Table 1) [59]. In this screen we incubated *cyfip2* wildtype, heterozygous, and mutant larvae in each compound for 30 min prior to and during acoustic startle testing. Consistent with previous findings, *N*-phenylanthrinilic acid (NPAA; Cl^- channel antagonist), Meclofenamic acid (MA; K^+ channel and gap junction antagonist), Phenoxybenzamine (POBA; alpha-adrenergic receptor and calmodulin antagonist), Etazolate (ETAZ; phosphodiesterase 4 (PDE4) inhibitor), and MK-801 (N-methyl-D-aspartate receptor (NMDAR) antagonist) all increased startle sensitivity in a dose-dependent manner (Table 1). BMS204352, a different K^+ channel antagonist, did not alter acoustic startle sensitivity at either 10 or 50 μM concentrations, and NSC-23766, a Rac1 antagonist, reduced sensitivity in siblings at 100 μM, but not *cyfip2* mutants.

Compound	Concentration (μM)	Effect By Genotype		
		cyfip2(+/+)	***cyfip2(+/-)***	***cyfip2(-/-)***
NPAA (Cl-channel antagonist)	1	93.21% of Control, p > 0.99	110.21% of Control, p < 0.99	113.57% of Control, p > 0.99
	5	140.11% of Control, p = 0.9785	137.32% of Control, p = 0.1385	140.29% of Control, p > 0.2787
	10	**234.14% of Control, p** = 0.0038**	**201.29% of Control, p**** < 0.0001**	**155.06% of Control, p* = 0.0189**
MA (K+ channel/gap jxn. antagonist)	1	131.6% of Control, p > 0.99	11.87% of Control, p > 0.99	132.29% of Control, p = 0.5732
	5	137.24% of Control, p > 0.99	138.46% of Control, p = 0.0622	112.29% of Control, p > 0.99
	10	214.13% of Control, p = 0.0833	**169.81% of Control, p* = 0.0188**	**155.76% of Control, p* = 0.0288**
POBA (AAR/calmodulin antagonist)	1	102.9% of Control, p > 0.99	107.08% of Control, p > 0.99	101.04% of Control, p > 0.99
	10	136.17% of Control, p > 0.99	106.58% of Control, p > 0.99	99.01% of Control, p > 0.99
	50	**175.8% of Control, p* = 0.0123**		99.76% of Control, p > 0.99
ETAZ (PDE4 inhibitor)	1	141.79% of Control, p > 0.99	126.36% of Control, p > 0.99	121.74% of Control, p > 0.99
	10	168.6% of Control, p = 0.5472	**172.26% of Control, p* = 0.0137**	152.73% of Control, p = 0.3977

	50	**236.64% of Control, p** = 0.0029**	**179.99% of Control, p** = 0.0015**	**149.75% of Control, p* = 0.0105**
MK-801 (NMDAR antagonist)	100	120.19% of Control, p > 0.99		**145.93% of Control, p** = 0.0024**
	500	**212.69% of Control, p**** < 0.0001**		**163.26% of Control, p*** = 0.0002**
BMS-204352 (K+ channel antagonist)	10	79.48% of Control, p = 0.4269		89.55% of Control, p > 0.99
	50	76.08% of Control, p = 0.6759		108.74% of Control, p > 0.99
NSC-23766 (Rac1 antagonist)	100	**49.14% of Control, p*** = 0.0002**		81.60% of Control, p > 0.99
	200	86.26% of Control, p > 0.99		105.28% of Control, p > 0.99

Table 1. Cyfip2 may regulate NMDARs to control acoustic startle sensitivity. Mean startle index comparisons, listed as percentage (%) of the mean startle index of vehicle-treated controls by *cyfip2* genotype and drug concentration, for larvae treated with compounds targeting the indicated pathways [59] to increase acoustic startle sensitivity. All significant differences ($p < 0.05$) are listed (**bold**) for comparisons using a Kruskal-Wallis test and Dunn's multiple comparisons correction. NPAA (*N*-phenylanthranilic acid); MA (meclofenamic acid); POBA (phenoxybenzamine); ETAZ (etazolate).

To determine whether any of the targeted pathways may be downstream of Cyfip2, we looked for conditions in which there was a clear *cyfip2* genotype-specific effect on sensitivity. The NMDA receptor blocker MK-801 showed the clearest such effect, with a low dose (100 μM) elevating startle sensitivity only in *cyfip2* mutants but not siblings (Table 1). Therefore, Cyfip2-mediated cytoskeletal and/or translational regulation may impact the expression and/or function of NMDA receptors within the startle circuit to modulate the acoustic startle threshold.

Proteomic analysis reveals that Cyfip2-mediated regulation of $GABA_B$ receptors is critical for startle sensitivity.

To complement our candidate drug screen with an unbiased approach to identify proteins and molecular pathways regulated by Cyfip2, likely through its role in translational regulation, we conducted a proteomic analysis of *cyfip2* wildtype, heterozygous, and mutant larvae at 5 dpf. All larvae used were siblings and were genotyped by PCR and Sanger sequencing and then pooled in groups of 30 per genotype and snap frozen with liquid nitrogen. Three independent pools of 30 larvae were analyzed for each genotype. Protein lysates were submitted to the Molecular Education, Technology and Research Innovation Center (METRIC)

at NC State University for protein digestion and LC-MS. Raw LC-MS files were processed and quantified using MaxQuant (Max Planck Institute of Biochemistry) and imported into Perseus software for transformation and identification of Differentially Expressed Proteins (DEPs) for subsequent Ingenuity Pathway Analysis (IPA).

Comparative analysis of *cyfip2* heterozygous and mutant versus wildtype proteomes identified a total of 221 differentially expressed proteins (DEPs) in heterozygotes and 127 DEPs in mutants (Fig. S5A-B; Tables S7,S8). Cyfip2 was the most strongly downregulated protein in mutants, providing a key validation of our approach (Fig. 3A,S5A; Tables S7,S8). Cyfip2 was slightly but significantly downregulated in heterozygotes as well (Fig. S5B), providing a basis for the sensitization of Cyfip2 heterozygotes to the actin inhibitor CK-869 (Fig. 2B). Cyfip1 expression was not significantly altered in either genotype, indicating that it likely does not act to compensate for the loss of Cyfip2 (Fig. S5A-B). 66 DEPs were shared between *cyfip2* heterozygotes and mutants, while 155 and 61 DEPs were specific to each group, respectively (Fig. S5C). The top 5 upregulated proteins identified in *cyfip2*^{p400} heterozygotes in descending order included: microtubule actin cross-linking factor 1 (MACF1), acyl-CoA dehydrogenase family member 11 (ACAD11), cullin 2 (CUL2), calcium channel, voltage dependent, L-type alpha 1S (CACNA1S) and ubiquitin specific peptidase 24 (USP24) (Fig. 3A; top, green). The top 5 downregulated proteins identified in *cyfip2*^{p400} heterozygotes in descending order included: tyrosine 3-monooxygenase/tryptophan 5-monooxygenase activation protein theta or 14-3-3 protein theta (YWHAQ), SEC61 translocon subunit alpha 1 (SEC61A1), ribosomal protein S5 (RPS5), enolase 2 (ENO2), and ribosomal protein L18A (RPL18A) (Fig 3A; top, red). The top 5 upregulated proteins identified in *cyfip2*^{p400} mutants in descending order included: ACAD11, mitochondrial NADH dehydrogenase 4 (MT-ND4), NIPBL cohesion loading factor b (NIPBL), troponin C2 fast skeletal type (TNNC2), and USP24 (Fig 3A; bottom, green). The top 5 downregulated proteins identified in *cyfip2*^{p400} mutants in descending order included: cytoplasmic FMR1-interacting protein 2 (CYFIP2), collagen type VI alpha 3 (COL6A3), stress-

366 induced phosphoprotein 1 (STIP1), thymosin beta (TMSB10/TMSB4X) and collagen type 1
367 alpha 1 (COL1A1) (Fig 3A; bottom, green). These changes highlight the diverse set of roles that
368 Cyfip2 plays, impacting translational machinery, metabolism, and the extracellular matrix.
369 IPA analysis of DEPs in *cyfip2* heterozygotes and mutants revealed disruption of
370 multiple pathways common to both genotypes. Notable disrupted pathways shared between
371 *cyfip2* heterozygotes and mutants include oxidative phosphorylation, mitochondrial dysfunction,
372 EIF2 signaling, sirtuin signaling, eIF4/p70S6K signaling, 14-3-3-mediated signaling, and GABA
373 receptor signaling (Fig. 3B). Analysis of the most affected diseases and functions for each
374 genotype supports a role for Cyfip2-mediated regulation in neuromuscular disease, disorder of
375 the basal ganglia, dyskinesia, Huntington disease, breast cancer, familial encephalopathy, and
376 neurological disorders (Fig. 3C). These data provide further evidence of the central importance
377 of Cyfip2 for neural function.
378 Finally, we sought to confirm that these pathways play a functional role in regulating
379 startle sensitivity, and so we focused on GABA receptor signaling as the likeliest to contribute to
380 the hyperexcitability of *cyfip2* mutant larvae. We applied agonists of both ionotropic $GABA_A$
381 receptors (muscimol) and metabotropic $GABA_B$ receptors (baclofen) for 1 hour prior to startle
382 testing. Muscimol did not have a consistent impact on mutant hypersensitivity at 1, 10, or 100
383 μM (Fig. 3D), but baclofen induced a clear restoration of normal sensitivity in *cyfip2* mutants at
384 10 μM (Fig. 3E). Importantly, baclofen application did not affect startle sensitivity in sibling
385 larvae. Thus, Cyfip2 maintains a normal startle threshold by promoting GABAergic inhibition
386 through the activity of $GABA_B$ receptors. Together our findings establish a set of molecular
387 pathways downstream of Cyfip2 that enable the proper processing of acoustic stimuli to limit
388 sensory over-responsiveness.
389

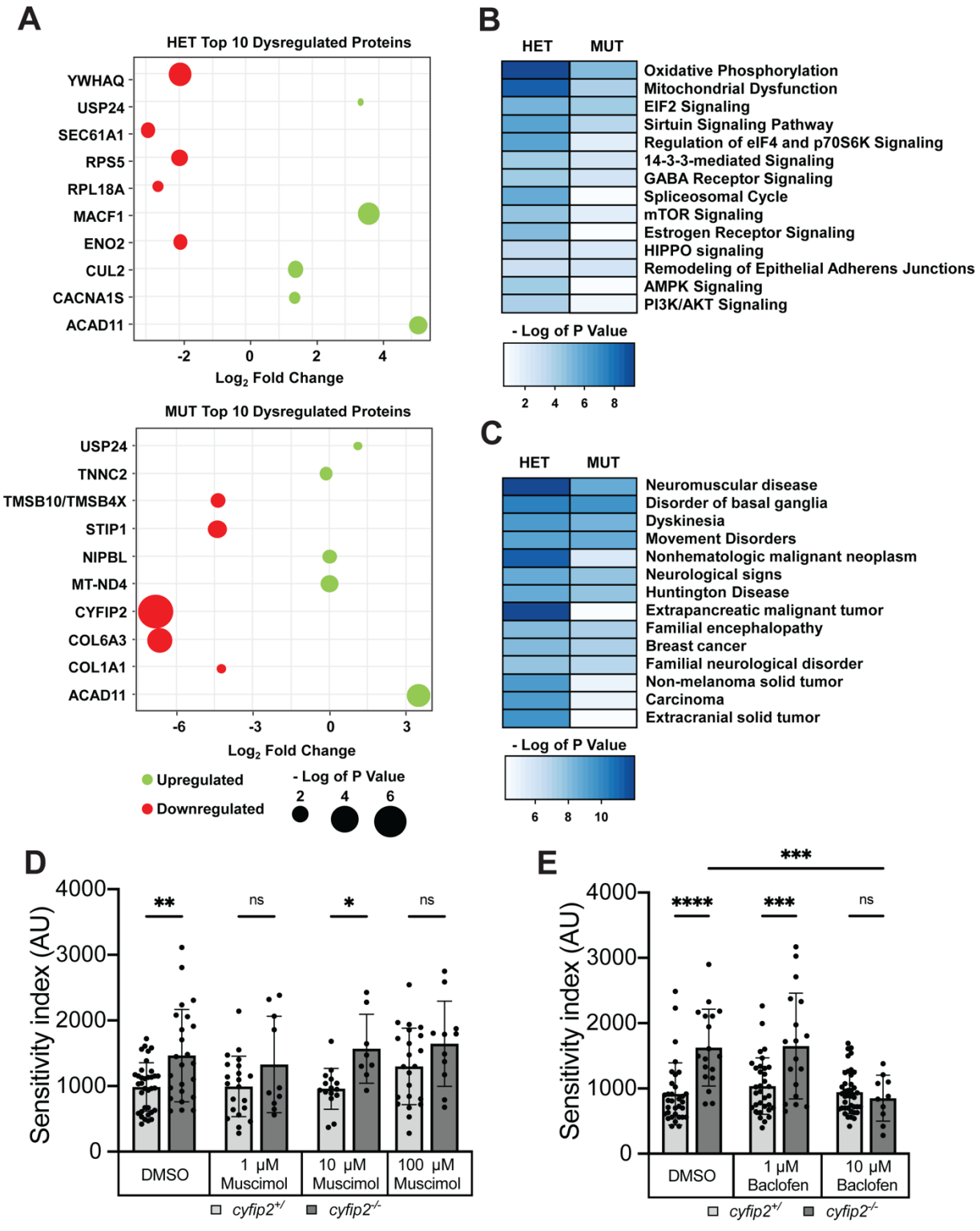

Figure 3. Loss of Cyfip2 causes widespread proteomic changes and $GABA_B$ receptor signaling is critical for startle sensitivity. (A) Bubble plots reporting the level of significance of the top 10 dysregulated proteins for both *cyfip2* heterozygous (top) and mutant (bottom) groups compared to wildtype controls. The size of the dot is proportional to the significance of the results while the color code represents the log_2 fold change; top five upregulated (green), and top five downregulated (red) proteins

are shown. (B-C) Heat maps displaying the impacted canonical pathways (B) and diseases and biological functions (C) from IPA functional analysis. The blue-colored gradient indicates the degree of enrichment for the listed pathways or diseases/functions, as represented by the – log of the P value for each pathway, disease and/or function. (D-E) Sensitivity indices for 5 dpf *cyfip2* sibling (+/) and mutant (-/-) larvae, treated for 60 minutes prior to testing with muscimol (D) or (E) baclofen. All indices (mean ± SD) were compared using a one-way ANOVA with Sidak's multiple comparisons correction. p* < 0.05, p** < 0.01; p*** < 0.001; p**** < 0.0001.

Discussion

Through its ability to modulate both the actin cytoskeleton and protein translation, Cyfip2 is well-positioned to be a critical factor for many processes in neurodevelopment [33,34,37–39,45,49]. Further highlighting its importance, Cyfip2 has been implicated in an array of neuropsychiatric and other conditions, including schizophrenia [60], autism [49,61–63], binge eating [64–66], obesity [67], amyotrophic lateral sclerosis (ALS) [68,69], Alzheimer's disease [70], epilepsy [63,71–74], and cancer [75–80]. Here we focused on Cyfip2's role in a common endophenotype of schizophrenia and autism, increased acoustic startle responsiveness [4,24,27,28]. By combining conditional transgenesis, CRISPR/Cas9 gene editing, pharmacology, and discovery proteomics in an *in vivo*, vertebrate model system, we found that both actin and translational regulation pathways are required for Cyfip2 to establish and maintain a normal startle threshold. Our data indicate that through these pathways Cyfip2 regulates both excitatory (NMDA receptor) and inhibitory ($GABA_B$ receptor) function to establish and maintain proper sensory responsiveness.

Cyfip2 acts through both Rac1 and FMRP to establish the acoustic startle threshold.

The actin regulating function of Cyfip2-Rac1 interactions is essential for many neurodevelopmental processes including neuronal outgrowth and maturation, synapse formation and function, axon guidance and cell migration [38,44,45,81]. The functional importance of Cyfip2-FMRP interactions, though less well characterized than Cyfip1-FMRP interactions, are thought to similarly impact the expression of many key neurodevelopmental

proteins that are directly involved in axon growth, synapse maturation, and synaptic plasticity [34,45,82–84]. Here we used a heatshock-inducible expression system to reveal that Cyfip2 requires the ability to interact with both Rac1 and FMRP to establish the acoustic startle threshold early in neurodevelopment (Fig. 1E). The ability of wildtype Cyfip2 to restore normal startle sensitivity in mutant larvae when expression is induced at 30 hpf (Fig. 1D,E), but not at 48, 72, or 96 hpf (Fig. S4) reveals some potential ways that it may affect the underlying neural circuits. Prior to the rescue window, by 8-15 hpf the command-like Mauthner cells have been specified [85] and begun extending their axons (17-18 hpf) and lateral dendrites (22-23 hpf) [86,87]. During the rescue window from ~30-48 hpf, other neurons in the startle circuit continue to migrate to their final positions in the ventral hindbrain, and the synaptic contacts within the circuit begin to form and mature, including those between the auditory nerve, Mauthner cells, and excitatory Spiral Fiber Neurons (SFNs) [87–89]. Actin dynamics would be required during this time to facilitate neuronal migration, axon and dendrite growth, and synapse formation. These processes would also require precisely regulated RNA translation through complexes like Cyfip2-FMRP-eIF4E to produce the many proteins needed to establish these connections. When we induced Cyfip2 expression at 5 dpf we observed a clear bimodal distribution with some mutants remaining hypersensitive and a second population with normal sensitivity (Fig. 2A). This pattern was not observed when Rac1 or FMRP binding was abolished, suggesting that both pathways are also needed for Cyfip2 to modulate the startle circuit in this acute context, which would likely occur through changes in neuronal and/or synaptic function rather than altered connectivity. That Cyfip2 expression between 48-96 hpf did not restore the startle threshold in mutants could be due to insufficient expression levels, but together our conditional expression experiments more likely indicate that Cyfip2 is able to most reliably function when the circuit is in a less mature state.

Our findings also show that Cyfip2-Rac1 but not Cyfip2-FMRP binding is required for the performance of the startle response, as kinematic parameters including latency, turn angle, and

duration were largely restored to normal by wildtype and Δ*FMRP* versions of Cyfip2 but remained altered in Δ*Rac1*-Cyfip2 expressing *cyfip2* mutants (Fig. S1). These data demonstrate that the actin regulation and translation regulation functions of Cyfip2, while both are required in some contexts, also have some non-overlapping roles. This is consistent with findings in zebrafish larvae showing that Cyfip2's interaction with FMRP is dispensable but that its interaction with the Wave Regulatory Complex (WRC), which like the Rac1-Cyfip2 interaction regulates actin polymerization (Fig. 1B), is required for retinal ganglion cell (RGC) axons to properly navigate to their targets in the contralateral optic tectum [45]. In the startle context, our data showing that Δ*FMRP*-Cyfip2 drives a stronger rescue for turn angle and duration than for latency suggest that the Cyfip2-FMRP translational regulation pathway contributes more to the initial sensory processing of acoustic stimuli than the regulation of motor output in the spinal cord. The actin regulatory function of Cyfip2, however, appears to be critical for all of Cyfip2's known roles in the startle circuit.

Cyfip2-dependent startle threshold regulation requires FMRP but not FXR1/2.

Previously, we observed that mutants from the *fmr1*^{hu2787} line have normal startle sensitivity, suggesting that FMRP plays no role in regulating the startle threshold [32]. So here we tested whether Cyfip2, which in contrast to the closely related Cyfip1 has the capacity to also bind with the Fragile X-related proteins FXR1 and FXR2 [33], may instead rely on these binding partners to modulate the startle threshold. Like FMRP, both FXR1 and FXR2 regulate RNA translation [90,91] and are expressed in the brain during early vertebrate neurodevelopment, though divergent expression patterns emerge for the FXR1/2 proteins in later development and adulthood in most vertebrates [92–94]. By analyzing FMRP, FXR1, and FXR2 crispants, however, we found that FXR1 and FXR2 are dispensable but that FMRP is required for normal startle sensitivity (Fig. 1F). This data is consistent with the distinct expression patterns of the FMRP, FXR1 and FXR2 proteins, as well as the inability of FXR1/2 to functionally compensate

for the loss of FMRP [92–94]. Similarly, in *Drosophila*, which have only one Fragile X protein family member (dFMR1), re-expressing human FMRP (hFMR1), but not human FXR1 or FXR2, in dFMR1 mutants is sufficient to specifically rescue aberrant neuronal phenotypes [95]. As discussed above, the fact that *fmr1* crispants but not *fmr1*^{hu2787} mutants show startle hypersensitivity likely is due to genomic adaptation in the ENU-induced *fmr1*^{hu2787} line [50]. Furthermore, we observed that *fmr1* crispants show even further increased startle sensitivity in the *cyfip2* mutant background compared to *cyfip2* mutants alone (Fig. 1F), strengthening our conclusion that Cyfip2 and FMRP work cooperatively to regulate the startle threshold.

Cyfip2-dependent branched actin dynamics are required for maintaining the acoustic startle threshold.

Our rescue experiments indicate that Cyfip2's actin regulatory function through its binding with Rac1 is required during startle circuit development (Fig. 1E) and that this pathway may also facilitate a more acute role for Cyfip2 in maintaining the startle threshold (Fig. 2A). This conclusion is bolstered by our finding that inhibition of Arp2/3 with 20 μM CK-869 for 30 minutes prior to testing uncovers startle hypersensitivity in *cyfip2* heterozygotes but not wildtypes (Fig. 2B). Thus in wildtypes, Cyfip2 must act acutely to facilitate actin polymerization to maintain the startle threshold in the face of this challenge. Arp2/3-mediated F-actin nucleation creates branched actin filaments, while formin-mediated nucleation produces unbranched filaments [54–56,96]. Our data show that only branched actin nucleation is required for acute maintenance of the startle threshold, while both formin activity and cofilin-mediated actin filament severing play no acute role in regulating the startle threshold (Fig. 2C). Formin 2B has been shown with morpholinos to be required developmentally for normal startle responsiveness, however, and it appears to play a role in the growth of Spiral Fiber Neuron (SFN) axons [58]. SFNs are excitatory interneurons that receive input from the contralateral auditory nerve and project their axons across the midline to the contralateral Mauthner cell, providing a key driving

force to initiate the startle response [97]. We previously found that SFNs, but not Mauthner cells, have heightened excitability in *cyfip2* mutants [32], making them a likely place for Cyfip2 to regulate the startle threshold. Functioning acutely, Cyfip2 may impact synaptic input onto SFNs, and it is possible that inhibitory and/or excitatory synapses may be affected by Cyfip2 to maintain the startle threshold. Cyfip1 and Cyfip2 are both enriched at excitatory synapses and regulate dendritic complexity and spine maturation in mouse cortical neurons [82,83]. Both Cyfip1 and Cyfip2 are also found at inhibitory postsynaptic sites in mouse hippocampal neurons, and overexpression of either protein disrupts excitatory/inhibitory (E/I) synaptic balance [84]. It is likely that Cyfip2 functions similarly in the zebrafish startle circuit to regulate neuronal excitability, as our data implicate both excitatory (NMDA receptors; Fig. 2D) and inhibitory (GABA receptors; Fig. 3B,E) pathways.

<u>Cyfip2 may control sensory processing and other disease-related functions by regulating neurotransmitter receptors, mitochondrial function, and/or cytoskeletal remodeling.</u>

Our candidate drug screen to identify potential downstream effectors of Cyfip2 in regulating the startle threshold builds on previous work showing that NMDA receptor function is required for normal startle sensitivity (Fig 2D; Table 1) [59]. While our screen confirmed the known roles of Cl^- and K^+ channels, gap junctions, calmodulin, and PDE4 in regulating startle sensitivity, only the NMDA receptor blocker MK-801 produced a *cyfip2* genotype-specific response, indicating that Cyfip2 may impact NMDA receptor expression and/or function in the startle circuit. Our unbiased proteomic analysis of *cyfip2* heterozygotes and mutants did not uncover dysregulation in excitatory synaptic function compared to wildtypes, although this may be because we analyzed protein lysates from whole larvae and thus may have diluted out any changes in NMDA receptor expression in specific neuronal subpopulations. It may also be the case that Cyfip2 modulates the membrane localization of NMDA receptors through actin-mediated trafficking rather than impacting total expression levels.

Ingenuity Pathway Analysis (IPA) of our proteomic data revealed that inhibitory GABA receptor signaling is significantly disrupted in *cyfip2* heterozygotes and mutants (Fig. 3B). This change most likely occurs through Cyfip2's translational regulation role via FMRP, although further experiments are required to determine where and how Cyfip2 affects GABA receptor expression. We did confirm that Cyfip2-mediated regulation of GABA receptor function plays a key functional role in the startle threshold, showing that activation of $GABA_B$ but not $GABA_A$ receptors is sufficient to rescue the startle hypersensitivity phenotype in *cyfip2* mutants (Fig. 3D,E). Critically, the concentration of baclofen used did not affect wildtypes, and *cyfip2* mutant startle sensitivity was reduced to the same level as in wildtypes, indicating that the rescue was not due to a sedative effect. This result is consistent with recent findings using rats in which baclofen-mediated activation of $GABA_B$ receptors restored normal auditory processing in *Cntnap2* knockout animals [98]. $GABA_B$ receptors function both pre-synaptically to regulate neurotransmitter release and post-synaptically to activate inward-rectifying K^+ channels that cause hyperpolarization [99,100]. $GABA_B$ receptors are also expressed at high levels throughout the auditory system [101], and baclofen treatment has been shown to improve social avoidance in some individuals with autism [102–104]. It is currently unknown whether baclofen affects sensory processing in clinical populations, however. Our data fit with a growing body of evidence that $GABA_B$ receptors are critical modulators of auditory function with direct clinical applications.

The most significantly disrupted pathways in our proteomic analysis of *cyfip2* heterozygotes and mutants were oxidative phosphorylation and mitochondrial dysfunction (Fig. 3B). It is unclear if these metabolic functions influence the activity of the acoustic startle circuit, although these pathways are essential within neurons for neuronal development and plasticity, cell death, axon extension and branching, and synaptogenesis [105,106], and so they may also contribute to the many disease associations for Cyfip2 listed above. Our data also show that in the absence of Cyfip2, mitochondrial proteins (ACAD11, MT-ND4) increase in abundance, and

555 cytoskeletal (TMSB10/TMSB4X) and extracellular matrix (ECM) proteins (COL6A3, COL1A1)
556 decrease in abundance (Fig 3A; Table S8). TMSB4X and TMSB10 both suppress actin
557 polymerization [107,108], so their downregulation in *cyfip2* mutants may reflect an attempt to
558 compensate for the loss of Cyfip2- and WRC-mediated actin polymerization. ECM collagens like
559 COL6A3 and COL1A1 are important for multiple aspects of neural development including axon
560 guidance [109,110], and so this may reflect another potential mechanism for Cyfip2's
561 developmental role in regulating the startle circuit. Our analysis of diseases and functions
562 impacted by the loss of Cyfip2 include multiple neurological and neuromuscular conditions (Fig.
563 3C). These findings reinforce the known associations between *cyfip2* and diseases like ALS
564 [68,69] and Alzheimer's disease [70], further underscoring the central importance of Cyfip2 for
565 neural function beyond the startle circuit. Further work is needed to more clearly define the links
566 between Cyfip2, its molecular effectors, and the development, function, and maintenance of
567 neural circuits in order to improve our understanding of and ability to treat these varied
568 conditions.
569

570 **Materials & Methods**

571 Zebrafish Husbandry and Maintenance

572 All animal use and procedures were approved by the North Carolina State University
573 Institutional Animal Care and Use Committee (IACUC). Zebrafish embryos were obtained from
574 the Zebrafish International Resource Center (ZIRC), the University of Pennsylvania, or
575 generated at North Carolina State University and raised in a recirculating housing system.
576 Animals were fed and housed at a 5 zebrafish/L density under a 14h:10h light-dark cycle at
577 28°C.

578 Embryos were generated by a male and female pair placed in a mating box
579 (Aquaneering) containing system water and artificial grass. The following morning, 2-3 hours
580 into the light cycle, embryos were collected in petri dishes containing E3 embryo media (5 mM

NaCl, 0.17 mM KCl, 0.33 mM CaCl2·2H2O, 0.33 mM MgSO4 in water). Embryos were examined under a brightfield compound microscope for fertilization and proper development and were kept in groups ≤ 65. Embryos were placed in a 29˚C incubator on a 14h:10h light-dark cycle. 50% of E3 media changed daily, and any embryos with gross morphological defects were removed and euthanized.

DNA Extraction & Genotyping

Fin biopsies were obtained from adult fish anesthetized in 0.02% Tricaine (MS-222; Fisher) in system water. Fin clips were taken using a razor blade to remove ~2-3 mm of tissue from the tail fin and samples were immediately fixed in 100% MeOH. Larval samples were individually fixed in 100% MeOH following behavioral testing. DNA was extracted using the HotShot DNA lysis method which consisted of a tissue lysis with base solution (25mM NaOH, 0.2mM EDTA), sample incubation at 95°C for 30 minutes, and sample neutralization with neutralizing solution (40mM Tris-HCl).*cyfip2*^{p400} fish were genotyped using rhAmp SNP Genotyping System (IDT). rhAmp SNP genotyping was carried out using *cyfip2* locus and allele specific primers (Table S3) targeting the wildtype and *cyfip2*^{p400} alleles. Genotyping for *Tg(hsp70:cyfip2-GFP), Tg(hsp70:cyfip2-(C179R)-GFP)* and *Tg(hsp70:cyfip2-(K723E)-GFP)* was accomplished by PCR amplification with primers specific to GFP (Table S4) followed by agarose gel electrophoresis.

Molecular Cloning

Alternative *cyfip2* rescue constructs (Δ*Rac1*; Δ*FMRP*) were generated from a pENTR *cyfip2*-EGFP plasmid [32] using custom primers and the Q5 Site Directed Mutagenesis Kit (NEB) to induce the desired C179R (Δ*Rac1*) and K723E (Δ*FMRP*) mutations. Mutagenesis was confirmed using restriction digest and Sanger sequencing (Table S3). LR Gateway Cloning (ThermoFisher) was used to insert the altered *cyfip2*-EGFPs into the pDEST I-SceI hsp70 destination vector. Transgenic lines were created by microinjection into 1-cell stage embryos

with a transgenesis mix containing phenol red, I-SceI enzyme, and the pDEST I-SceI hsp70:*cyfip2*-(C179R)-EGFP or pDEST I-SceI hsp70:*cyfip2*-(K723E)-EGFP plasmid.

Inducible Heatshock Rescue & Imaging

Inducible expression of *cyfip2-EGFP,* as well as C179R and K723E variants, was initiated at 30 hpf by placing dechorionated larvae into 96-well plates and incubating at 38°C for 15 or 40 minutes [32]. Following heatshock, larvae were returned to Petri dishes, and given 4 days of recovery at 29°C. GFP fluorescence was confirmed between 4-6 hours post-heatshock for startle experiments using a Nikon SMZ25 stereo microscope with a GFP bandpass filter and Lumen 200 fluorescence illumination system. For day 5 heatshock rescue experiments, larvae were given 4 hours of recovery at 29°C prior to startle sensitivity testing.

For imaging experiments, larvae were treated as above for transgene expression at 30 hpf and at 29°C for 1 hour recovered in petri dishes in groups ≤ 65. After 1 hour of recovery fluorescence was verified, and larvae were visualized using the stereo microscope system described above and larval images were captured at 1-, 3-, 6-, 18-, 24-, 30-, and 42-hours post-heatshock using a Nikon DS-Qi2 monochrome microscope camera. Image analysis was conducted using FIJI (ImageJ) analysis software to manually define ROIs encompassing the entire larval body, excluding the eye and auto fluorescent yolk sac. Fluorescence intensity values reflect the mean gray values recorded for respective ROIs.

Chemical Exposures

For all exposures, groups of 10-20 larvae (5 dpf) were incubated for specified periods of between 30 minutes and 16 hours within 35 mm Petri dishes in 2 mL of each drug solution. Drug solutions remained on larvae during startle testing for 30 minutes to 1-hour exposures. For 16-hour incubations larvae first received fresh E3 prior to testing. Following incubation, larvae were placed on the 6x6 acrylic testing grid and run through the acoustic startle assay. CK-869, CK-666, MK-801, *N*-phenylanthranilic acid (NPAA), meclofenamic acid (MA), phenoxybenzamine (POBA), etazolate (ETAZ), BMS 204352, muscimol, and baclofen were

obtained from Sigma-Aldrich. SMIFH2, IPA-3, GSK429286 and NSC23766 were acquired from Tocris through Fisher Scientific.

Behavioral Assays

All larvae were tested at 5 days post-fertilization (dpf) unless otherwise stated. On the day of testing, embryos were thoroughly screened for developmental defects, and those with gross morphological defects were removed prior to behavior testing. *cyfip2*^{p400} larvae without inflated swim bladders were not discarded, as *cyfip2* mutant larvae fail to inflate their swim bladders [32]. Larvae were adapted to the testing arena lighting and temperature conditions for 30 minutes prior to testing. As previously described, the behavioral testing system consists of a 36-well acrylic grid attached to an acoustic-vibrational shaker (Bruel-Kjaer), a photron mini UX-50 camera, LED lighting, InfraRed illuminator, and an acrylic IR diffuser [5,32,59].

To test the acoustic startle response, 5 dpf larvae were presented with 60 total stimuli with a 20 second interstimulus interval (ISI), with 10 pseudo randomized trials at each of the following 6 stimulus intensities: 13.6, 25.7, 29.2, 35.5, 39.6 and 53.6 dB. All stimuli were calibrated using a PCB Piezotronics accelerometer (#355B04) and signal conditioner (#482A21), and voltage outputs were converted to dB using the formula dB = 20 log (V/0.775) [32].

Behavioral Analysis

All responses in the acoustic startle assay were tracked using FLOTE analysis software [5,32,59]. Short latency C-bends (SLCs) were identified by FLOTE using defined kinematic parameters (latency, turn angle, duration, and maximum angular velocity). Startle sensitivity was calculated by measuring the SLC frequency at each of the six stimulus intensities during the 60-stimulus startle assay. Sensitivity indices were defined as the area under the startle frequency vs. stimulus intensity curve calculated using Prism software (GraphPad).

Larval Sample Preparation for Proteomics.

Larvae from incrosses of *cyfip2*$^{+/p400}$ carriers were raised as described above. At 3 dpf, DNA was extracted from larvae using the Zebrafish Embryonic Genotyping (ZEG) apparatus (DanioLab). ZEG samples were used for PCR amplification and then submitted for Sanger sequencing to determine the genotype at the *cyfip2*^{p400} locus. At 5 dpf larvae were sorted into pools of 30 larvae for each genotype: homozygous wild type, *cyfip2*^{p400} heterozygous, and homozygous mutant. Samples were snap frozen in liquid nitrogen and stored at -80˚C. They were then resuspended and lysed in 100 µL ammonium bicarbonate (ABC; pH 8) containing 1% sodium deoxycholate (SDC) using a Branson SLPe Sonicator (40:0.15;4C) delivering two 20 second pulses at 20% amplitude intensity separated by 10 seconds between pulses. Lysates were centrifuged at 10,000 rpm for 5 minutes at 4˚C, and the supernatants were retained and quantified using Pierce BCA protein quantification (ThermoFisher; Cat #: 23225) and an IMPLEN NP80 nanophotometer. Lysates were submitted the same-day to the Molecular Education, Technology and Research Innovation Center (METRIC) at NC State University for protein digestion and LC-MS.

Protein Digestion and LC-MS

Each lysed sample was normalized to 200 µg of protein in 200 µL of ABC/SDC solution. Disulfide reduction was conducted by adding 15 µL 50 mM DTT and incubating at 56˚C for 30 minutes. 200 µL of 8M urea in 0.1 M Tris buffer (pH 8) was added and samples were transferred to Vivicon 30kD Molecular Weight Cut-off (MWCO) filters. Samples were centrifuged at 12,000 x g for 10 minutes at 21˚C. 200 µL of 8 M urea in 0.1 M Tris buffer (pH 8) was added to the top of each filter, as well as 64 µL 55 mM iodoacetamide (IAA) solution and samples were incubated for 1 hour in the dark at room temperature. Samples were centrifuged at 12,000 x g for 20 minutes. 100 µL of 2 M urea, 10 mM $CaCl_2$ in 0.1 M Tris buffer (pH 8) was added and samples were centrifuged at 12,000 x g for 20 minutes. The previous step was repeated twice. 100 µL of 0.1 M Tris buffer (pH 7.5) was added and samples were centrifuged at 12,000 x g for 20-45 minutes. This step was repeated twice, with a 1-hour centrifuge period on the final spin. 200 µL

683 of 0.02 µg/mL trypsin in 0.1 M Tris buffer (pH 7.5) was added, and samples incubated overnight
684 at 37˚C. Following protein digestion with trypsin, samples were placed into fresh microcentrifuge
685 reservoirs, and 50 µL of quench solution (0.001% zwittergent3-16 in water, 1% formic acid) was
686 added and samples centrifuged at 12,000 x g for 1 hour. 450 µL quench solution was applied to
687 each filter and samples were centrifuged at 14,000 x g for 1 hour. Solutions were dried using a
688 speedvac concentrator and samples were stored dry until LC-MS. Samples were reconstituted
689 in 100 µL of mobile phase A (98% water, 2% acetonitrile, 0.1% formic acid) and peptides were
690 quantified via Pierce BCA assay. Samples were normalized to the lowest peptide concentration
691 for every sample and nanoLC-MS was conducted using a Thermo Orbitrap Exploris 480. This
692 work was performed in part by METRIC at NC State University, which is supported by the State
693 of North Carolina.

694 Proteomics data analysis

695 Shotgun proteomics raw files were processed and quantified with MaxQuant (version 2.2.0.0).
696 Briefly, the built-in Andromeda search engine scored MS2 spectra against fragment masses of
697 tryptic peptides derived from a *Danio rerio* reference proteome containing 93,351 entries
698 including isoforms (UniProt, accessed March 22, 2019). Our database search required variable
699 modifications (methionine oxidation and N-terminal acetylation) and a fixed modification
700 (cysteine carbamido-methylation) along with a minimum peptide length of 7 amino acids and
701 limited the search space to a maximum peptide mass of 4600 Da and a maximum of two missed
702 cleavages. The false discovery rate was controlled with a target-decoy approach at less than
703 1% for peptide spectrum matches and protein group identifications.

704 Bioinformatics

705 Label-Free quantification (LFQ) intensities from MaxQuant were imported into Perseus software
706 (version 2.0.7.0) and transformed to logarithmic scale with base two. Missing values were

replaced with values from the normal distribution, reducing the distributions to a factor of "0.3" (width) and down-shifting by "1.8" standard deviations while simulating random values to replace the missing values. This protein quantification was used to measure the fold-enrichment between *cyfip2*^{p400} heterozygous/homozygous and *cyfip2* wildtype groups. Statistical significance was calculated using a two-way Student t-test and FPR ($p<0.05$). Differentially expressed proteins (DEPs) were submitted to ingenuity pathway analysis (IPA) to identify their function, specific processes, and related enriched pathways/diseases.

Statistical Methods

All statistical analyses were performed using Prism (GraphPad). All data sets were tested for normality in Prism. Subsequent parametric or non-parametric tests and post-hoc analyses were performed using Prism, and significance values ($p < 0.05$) were reported.

Acknowledgements

We would like to thank Leonard Collins and Taufika Williams from METRIC at NC State University for their assistance with proteomic analysis. A special thank you to Kimberly Scofield and Kara Carlson for proofreading the manuscript.

Funding Disclosure

We are grateful for financial support from the National Institute for Neurological Disease and Stroke (R01-NS116354 to K.C.M.) and for seed funds provided by North Carolina State University's Center for Human Health and the Environment (CHHE) through a National Institute of Environmental Health Science center grant (P30 ES025128).

Competing Interests

The authors declare that no competing interests exist.

References

1. Burgess HA, Granato M. Modulation of locomotor activity in larval zebrafish during light adaptation. J Exp Biol. 2007;210: 2526–2539. doi:10.1242/jeb.003939

2. Vagnoni E, Lourenco SF, Longo MR. Threat modulates perception of looming visual stimuli. Curr Biol. 2012;22: R826-7. doi:10.1016/j.cub.2012.07.053

3. Randlett O, Haesemeyer M, Forkin G, Shoenhard H, Schier AF, Engert F, et al. Distributed Plasticity Drives Visual Habituation Learning in Larval Zebrafish. Curr Biol. 2019;29: 1337-1345.e4. doi:10.1016/j.cub.2019.02.039

4. Geyer MA, Swerdlow NR, Mansbach RS, Braff DL. Startle response models of sensorimotor gating and habituation deficits in schizophrenia. Brain Res Bull. 1990;25: 485–498. doi:10.1016/0361-9230(90)90241-q

5. Burgess HA, Granato M. Sensorimotor gating in larval zebrafish. J Neurosci. 2007;27: 4984–4994. doi:27/18/4984 [pii]

6. Weidenmüller A, Kleineidam C, Tautz J. Collective control of nest climate parameters in bumblebee colonies. Anim Behav. 2002;63: 1065–1071. doi:10.1006/anbe.2002.3020

7. Weidenmuller A. The control of nest climate in bumblebee (Bombus terrestris) colonies: interindividual variability and self reinforcement in fanning response. Behav Ecol. 2004;15: 120–128. doi:10.1093/beheco/arg101

8. Ward AJW, Sumpter DJT, Couzin ID, Hart PJB, Krause J. Quorum decision-making facilitates information transfer in fish shoals. Proc Natl Acad Sci U S A. 2008;105: 6948–6953. doi:10.1073/pnas.0710344105

9. Cresci A, De Rosa R, Agnisola C. Assessing the Influence of Personality on Sensitivity to Magnetic Fields in Zebrafish. J Vis Exp. 2019. doi:10.3791/59229

10. Michel WC, Sanderson MJ, Olson JK, Lipschitz DL. Evidence of a novel transduction pathway mediating detection of polyamines by the zebrafish olfactory system. J Exp Biol. 2003;206: 1697–1706. doi:10.1242/jeb.00339

11. Dudova I, Vodicka J, Havlovicova M, Sedlacek Z, Urbanek T, Hrdlicka M. Odor detection threshold, but not odor identification, is impaired in children with autism. Eur Child Adolesc Psychiatry. 2011;20: 333–340. doi:10.1007/s00787-011-0177-1

12. Tavassoli T, Baron-Cohen S. Olfactory detection thresholds and adaptation in adults with autism spectrum condition. J Autism Dev Disord. 2012;42: 905–909. doi:10.1007/s10803-011-1321-y

13. Takahashi H, Tsuboi A. Olfactory avoidance test (mouse). Bio Protoc. 2017;7: e2153. doi:10.21769/BioProtoc.2153

14. Blakemore S-J, Tavassoli T, Calò S, Thomas RM, Catmur C, Frith U, et al. Tactile sensitivity in Asperger syndrome. Brain Cogn. 2006;61: 5–13. doi:10.1016/j.bandc.2005.12.013

15. Kohashi T, Oda Y. Initiation of Mauthner- or non-Mauthner-mediated fast escape evoked by different modes of sensory input. J Neurosci. 2008;28: 10641–10653. doi:10.1523/JNEUROSCI.1435-08.2008

16. DeLorey TM, Sahbaie P, Hashemi E, Li W-W, Salehi A, Clark DJ. Somatosensory and sensorimotor consequences associated with the heterozygous disruption of the autism candidate gene, Gabrb3. Behav Brain Res. 2011;216: 36–45. doi:10.1016/j.bbr.2010.06.032

17. Puts NAJ, Wodka EL, Tommerdahl M, Mostofsky SH, Edden RAE. Impaired tactile processing in children with autism spectrum disorder. J Neurophysiol. 2014;111: 1803–1811. doi:10.1152/jn.00890.2013

18. Armington JC. The electroretinogram, the visual evoked potential, and the area-luminance relation. Vision Res. 1968;8: 263–276. doi:10.1016/0042-6989(68)90014-x

19. Campbell FW, Maffei L. The influence of spatial frequency and contrast on the perception of moving patterns. Vision Res. 1981;21: 713–721. doi:10.1016/0042-6989(81)90080-8

20. Yilmaz M, Meister M. Rapid innate defensive responses of mice to looming visual stimuli. Curr Biol. 2013;23: 2011–2015. doi:10.1016/j.cub.2013.08.015

21. Wang Y, Wu W, Zhang X, Hu X, Li Y, Lou S, et al. A Mouse Model of Visual Perceptual Learning Reveals Alterations in Neuronal Coding and Dendritic Spine Density in the Visual Cortex. Front Behav Neurosci. 2016;10: 42. doi:10.3389/fnbeh.2016.00042

22. Bakker MJ, Tijssen MA, van der Meer JN, Koelman JH, Boer F. Increased whole-body auditory startle reflex and autonomic reactivity in children with anxiety disorders. J Psychiatry Neurosci. 2009;34: 314–322. Available: https://www.ncbi.nlm.nih.gov/pubmed/19568483

23. Han K, Chen H, Gennarino VA, Richman R, Lu H-C, Zoghbi HY. Fragile X-like behaviors and abnormal cortical dendritic spines in cytoplasmic FMR1-interacting protein 2-mutant mice. Hum Mol Genet. 2015;24: 1813–1823. doi:10.1093/hmg/ddu595

24. Takahashi H, Nakahachi T, Stickley A, Ishitobi M, Kamio Y. Relationship between physiological and parent-observed auditory over-responsiveness in children with typical development and those with autism spectrum disorders. Autism. 2018;22: 291–298. doi:10.1177/1362361316680497 [doi]

25. Grillon C, Ameli R, Goddard A, Woods SW, Davis M. Baseline and fear-potentiated startle in panic disorder patients. Biol Psychiatry. 1994;35: 431–439. doi:10.1016/0006-3223(94)90040-x

26. Grillon C, Davis M. Acoustic startle and anticipatory anxiety in humans: effects of monaural right and left ear stimulation. Psychophysiology. 1995;32: 155–161. doi:10.1111/j.1469-8986.1995.tb03307.x [doi]

27. Chamberlain PD, Rodgers J, Crowley MJ, White SE, Freeston MH, South M. A potentiated startle study of uncertainty and contextual anxiety in adolescents diagnosed with autism spectrum disorder. Mol Autism. 2013;4: 31. doi:10.1186/2040-2392-4-31

28. Kohl S, Heekeren K, Klosterkötter J, Kuhn J. Prepulse inhibition in psychiatric disorders--apart from schizophrenia. J Psychiatr Res. 2013;47: 445–452. doi:10.1016/j.jpsychires.2012.11.018

29. Eaton RC, Bombardieri RA, Meyer DL. The Mauthner-initiated startle response in teleost fish. J Exp Biol. 1977;66: 65–81. doi:10.1242/jeb.66.1.65

30. Kimmel CB, Patterson J, Kimmel RO. The development and behavioral characteristics of the startle response in the zebra fish. Dev Psychobiol. 1974;7: 47–60. doi:10.1002/dev.420070109

31. Davis M, Gendelman DS, Tischler MD, Gendelman PM. A primary acoustic startle circuit: lesion and stimulation studies. J Neurosci. 1982;2: 791–805. doi:10.1523/JNEUROSCI.02-06-00791.1982

32. Marsden KC, Jain RA, Wolman MA, Echeverry FA, Nelson JC, Hayer KE, et al. A Cyfip2-Dependent Excitatory Interneuron Pathway Establishes the Innate Startle Threshold. Cell Rep. 2018;23: 878–887. doi:S2211-1247(18)30471-6 [pii]

33. Schenck A, Bardoni B, Moro A, Bagni C, Mandel JL. A highly conserved protein family interacting with the fragile X mental retardation protein (FMRP) and displaying selective interactions with FMRP-related proteins FXR1P and FXR2P. Proc Natl Acad Sci U S A. 2001;98: 8844–8849. doi:10.1073/pnas.151231598 [doi]

34. Napoli I, Mercaldo V, Boyl PP, Eleuteri B, Zalfa F, Rubeis SD, et al. The fragile X syndrome protein represses activity-dependent translation through CYFIP1, a new 4E-BP. Cell. 2008;134: 1042–1054. doi:10.1016/j.cell.2008.07.031 [doi]

35. Kobayashi K, Kuroda S, Fukata M, Nakamura T, Nagase T, Nomura N, et al. p140Sra-1 (specifically Rac1-associated protein) is a novel specific target for Rac1 small GTPase. J Biol Chem. 1998;273: 291–295. doi:10.1074/jbc.273.1.291 [doi]

36. Eden S, Rohatgi R, Podtelejnikov AV, Mann M, Kirschner MW. Mechanism of regulation of WAVE1-induced actin nucleation by Rac1 and Nck. Nature. 2002;418: 790–793. doi:10.1038/nature00859

37. Schenck A, Bardoni B, Langmann C, Harden N, Mandel JL, Giangrande A. CYFIP/Sra-1 controls neuronal connectivity in Drosophila and links the Rac1 GTPase pathway to the fragile X protein. Neuron. 2003;38: 887–898. doi:S0896627303003544 [pii]

38. Bogdan S, Grewe O, Strunk M, Mertens A, Klämbt C. Sra-1 interacts with Kette and Wasp and is required for neuronal and bristle development in Drosophila. Development. 2004;131: 3981–3989. doi:10.1242/dev.01274

39. Chen Z, Borek D, Padrick SB, Gomez TS, Metlagel Z, Ismail AM, et al. Structure and control of the actin regulatory WAVE complex. Nature. 2010;468: 533–538. doi:10.1038/nature09623 [doi]

40. Chen B, Padrick SB, Henry L, Rosen MK. Biochemical reconstitution of the WAVE regulatory complex. Methods Enzymol. 2014;540: 55–72. doi:10.1016/B978-0-12-397924-7.00004-2

41. Chen B, Chou HT, Brautigam CA, Xing W, Yang S, Henry L, et al. Rac1 GTPase activates the WAVE regulatory complex through two distinct binding sites. Elife. 2017;6: 10.7554/eLife.29795. doi:10.7554/eLife.29795 [doi]

42. Trowe T, Klostermann S, Baier H, Granato M, Crawford AD, Grunewald B, et al. Mutations disrupting the ordering and topographic mapping of axons in the retinotectal projection of the zebrafish, Danio rerio. Development. 1996;123: 439–450. doi:10.1242/dev.123.1.439

43. Schenck A, Qurashi A, Carrera P, Bardoni B, Diebold C, Schejter E, et al. WAVE/SCAR, a multifunctional complex coordinating different aspects of neuronal connectivity. Dev Biol. 2004;274: 260–270. doi:10.1016/j.ydbio.2004.07.009

44. Pittman AJ, Gaynes JA, Chien CB. Nev (Cyfip2) is Required for Retinal Lamination and Axon Guidance in the Zebrafish Retinotectal System. Dev Biol. 2010;344: 784–794. doi:10.1016/j.ydbio.2010.05.512 [doi]

45. Cioni JM, Wong HH, Bressan D, Kodama L, Harris WA, Holt CE. Axon-Axon Interactions Regulate Topographic Optic Tract Sorting via CYFIP2-Dependent WAVE Complex Function. Neuron. 2018;97: 1078-1093.e6. doi:S0896-6273(18)30052-7 [pii]

46. Lee Y, Kim D, Ryu JR, Zhang Y, Kim S, Kim Y, et al. Phosphorylation of CYFIP2, a component of the WAVE-regulatory complex, regulates dendritic spine density and neurite outgrowth in cultured hippocampal neurons potentially by affecting the complex assembly. Neuroreport. 2017;28: 749–754. doi:10.1097/WNR.0000000000000838

47. Zhang Y, Kang Hyae R, Lee S-H, Kim Y, Ma R, Jin C, et al. Enhanced Prefrontal Neuronal Activity and Social Dominance Behavior in Postnatal Forebrain Excitatory Neuron-Specific Cyfip2 Knock-Out Mice. Front Mol Neurosci. 2020;13: 574947. doi:10.3389/fnmol.2020.574947

48. Kumar V, Kim K, Joseph C, Kourrich S, Yoo SH, Huang HC, et al. C57BL/6N mutation in cytoplasmic FMRP interacting protein 2 regulates cocaine response. Science. 2013;342: 1508–1512. doi:10.1126/science.1245503 [doi]

49. Abekhoukh S, Bardoni B. CYFIP family proteins between autism and intellectual disability: links with Fragile X syndrome. Front Cell Neurosci. 2014;8: 81. doi:10.3389/fncel.2014.00081 [doi]

50. Barthelson K, Baer L, Dong Y, Hand M, Pujic Z, Newman M, et al. Zebrafish chromosome 14 gene differential expression in the fmr1 h u2787 model of Fragile X syndrome. Front Genet. 2021;12: 625466. doi:10.3389/fgene.2021.625466

880 51. Hu J, Chen L, Yin J, Yin H, Huang Y, Tian J. Hyperactivity, memory defects, and
881 craniofacial abnormalities in zebrafish fmr1 mutant larvae. Behav Genet. 2020;50: 152–
882 160. doi:10.1007/s10519-020-09995-7

883 52. Spence EF, Soderling SH. Actin Out: Regulation of the Synaptic Cytoskeleton. J Biol
884 Chem. 2015;290: 28613–28622. doi:10.1074/jbc.R115.655118 [doi]

885 53. Chalkia D, Nikolaidis N, Makalowski W, Klein J, Nei M. Origins and evolution of the formin
886 multigene family that is involved in the formation of actin filaments. Mol Biol Evol. 2008;25:
887 2717–2733. doi:10.1093/molbev/msn215

888 54. Pellegrin S, Mellor H. The Rho family GTPase Rif induces filopodia through mDia2. Curr
889 Biol. 2005;15: 129–133. doi:10.1016/j.cub.2005.01.011

890 55. Schirenbeck A, Bretschneider T, Arasada R, Schleicher M, Faix J. The Diaphanous-related
891 formin dDia2 is required for the formation and maintenance of filopodia. Nat Cell Biol.
892 2005;7: 619–625. doi:10.1038/ncb1266

893 56. Peng J, Wallar BJ, Flanders A, Swiatek PJ, Alberts AS. Disruption of the Diaphanous-
894 related formin Drf1 gene encoding mDia1 reveals a role for Drf3 as an effector for Cdc42.
895 Curr Biol. 2003;13: 534–545. doi:10.1016/s0960-9822(03)00170-2

896 57. Maciver SK, Hussey PJ. The ADF/cofilin family: actin-remodeling proteins. Genome Biol.
897 2002;3: reviews3007. doi:10.1186/gb-2002-3-5-reviews3007

898 58. Nagar D, James TK, Mishra R, Guha S, Burgess SM, Ghose A. The Formin Fmn2b Is
899 Required for the Development of an Excitatory Interneuron Module in the Zebrafish
900 Acoustic Startle Circuit. eNeuro. 2021;8. doi:10.1523/ENEURO.0329-20.2021

901 59. Wolman MA, Jain RA, Liss L, Granato M. Chemical modulation of memory formation in
902 larval zebrafish. Proc Natl Acad Sci U S A. 2011;108: 15468–15473.
903 doi:10.1073/pnas.1107156108 [doi]

904 60. Focking M, Lopez LM, English JA, Dicker P, Wolff A, Brindley E, et al. Proteomic and
905 genomic evidence implicates the postsynaptic density in schizophrenia. Mol Psychiatry.
906 2015;20: 424–432. doi:10.1038/mp.2014.63 [doi]

907 61. Hoeffer CA, Sanchez E, Hagerman RJ, Mu Y, Nguyen DV, Wong H, et al. Altered mTOR
908 signaling and enhanced CYFIP2 expression levels in subjects with fragile X syndrome.
909 Genes Brain Behav. 2012;11: 332–341. doi:10.1111/j.1601-183X.2012.00768.x [doi]

910 62. Noroozi R, Omrani MD, Sayad A, Taheri M, Ghafouri-Fard S. Cytoplasmic FMRP
911 interacting protein 1/2 (CYFIP1/2) expression analysis in autism. Metab Brain Dis. 2018;33:
912 1353–1358. doi:10.1007/s11011-018-0249-8 [doi]

913 63. Zweier M, Begemann A, McWalter K, Cho MT, Abela L, Banka S, et al. Spatially clustering
914 de novo variants in CYFIP2, encoding the cytoplasmic FMRP interacting protein 2, cause
915 intellectual disability and seizures. Eur J Hum Genet. 2019;27: 747–759.
916 doi:10.1038/s41431-018-0331-z

64. Kirkpatrick SL, Goldberg LR, Yazdani N, Babbs RK, Wu J, Reed ER, et al. Cytoplasmic FMR1-Interacting Protein 2 Is a Major Genetic Factor Underlying Binge Eating. Biol Psychiatry. 2017;81: 757–769. doi:10.1016/j.biopsych.2016.10.021

65. Babbs RK, Beierle JA, Ruan QT, Kelliher JC, Chen MM, Feng AX, et al. Cyfip1 Haploinsufficiency Increases Compulsive-Like Behavior and Modulates Palatable Food Intake in Mice: Dependence on Cyfip2 Genetic Background, Parent-of Origin, and Sex. G3 . 2019;9: 3009–3022. doi:10.1534/g3.119.400470

66. Babbs RK, Beierle JA, Yao EJ, Kelliher JC, Medeiros AR, Anandakumar J, et al. The effect of the demyelinating agent cuprizone on binge-like eating of sweetened palatable food in female and male C57BL/6 substrains. Appetite. 2020;150: 104678. doi:10.1016/j.appet.2020.104678

67. Manigandan S, Yun JW. Loss of cytoplasmic FMR1-interacting protein 2 (CYFIP2) induces browning in 3T3-L1 adipocytes via repression of GABA-BR and activation of mTORC1. J Cell Biochem. 2022;123: 863–877. doi:10.1002/jcb.30231

68. Nachmany H, Wald S, Abekasis M, Bulvik S, Weil M. Two potential biomarkers identified in mesenchymal stem cells and leukocytes of patients with sporadic amyotrophic lateral sclerosis. Dis Markers. 2012;32: 211–220. doi:10.3233/DMA-2011-0885

69. Lilo E, Wald-Altman S, Solmesky LJ, Ben Yaakov K, Gershoni-Emek N, Bulvik S, et al. Characterization of human sporadic ALS biomarkers in the familial ALS transgenic mSOD1(G93A) mouse model. Hum Mol Genet. 2013;22: 4720–4725. doi:10.1093/hmg/ddt325

70. Tiwari SS, Mizuno K, Ghosh A, Aziz W, Troakes C, Daoud J, et al. Alzheimer-related decrease in CYFIP2 links amyloid production to tau hyperphosphorylation and memory loss. Brain. 2016;139: 2751–2765. doi:10.1093/brain/aww205

71. Nakashima M, Kato M, Aoto K, Shiina M, Belal H, Mukaida S, et al. De novo hotspot variants in CYFIP2 cause early-onset epileptic encephalopathy. Ann Neurol. 2018;83: 794–806. doi:10.1002/ana.25208 [doi]

72. Begemann A, Sticht H, Begtrup A, Vitobello A, Faivre L, Banka S, et al. New insights into the clinical and molecular spectrum of the novel CYFIP2-related neurodevelopmental disorder and impairment of the WRC-mediated actin dynamics. Genet Med. 2021;23: 543–554. doi:10.1038/s41436-020-01011-x

73. Biembengut ÍV, Silva ILZ, Souza T de ACB de, Shigunov P. Cytoplasmic FMR1 interacting protein (CYFIP) family members and their function in neural development and disorders. Mol Biol Rep. 2021;48: 6131–6143. doi:10.1007/s11033-021-06585-6

74. Biembengut ÍV, Shigunov P, Frota NF, Lourenzoni MR, de Souza TACB. Molecular Dynamics of CYFIP2 Protein and Its R87C Variant Related to Early Infantile Epileptic Encephalopathy. Int J Mol Sci. 2022;23. doi:10.3390/ijms23158708

75. Takahashi H, Nemoto T, Yoshida T, Honda H, Hasegawa T. Cancer diagnosis marker extraction for soft tissue sarcomas based on gene expression profiling data by using

projective adaptive resonance theory (PART) filtering method. BMC Bioinformatics. 2006;7: 399. doi:10.1186/1471-2105-7-399

76. Mongroo PS, Noubissi FK, Cuatrecasas M, Kalabis J, King CE, Johnstone CN, et al. IMP-1 displays cross-talk with K-Ras and modulates colon cancer cell survival through the novel proapoptotic protein CYFIP2. Cancer Res. 2011;71: 2172–2182. doi:10.1158/0008-5472.CAN-10-3295

77. Jiao S, Li N, Cai S, Guo H, Wen Y. Inhibition of CYFIP2 promotes gastric cancer cell proliferation and chemoresistance to 5-fluorouracil through activation of the Akt signaling pathway. Oncol Lett. 2017;13: 2133–2140. doi:10.3892/ol.2017.5743

78. Vandamme T, Beyens M, Boons G, Schepers A, Kamp K, Biermann K, et al. Hotspot DAXX, PTCH2 and CYFIP2 mutations in pancreatic neuroendocrine neoplasms. Endocr Relat Cancer. 2019;26: 1–12. doi:10.1530/ERC-18-0120

79. Liu Y, Liu H, Bian Q. Identification of Potential Biomarkers Associated with Basal Cell Carcinoma. Biomed Res Int. 2020;2020: 2073690. doi:10.1155/2020/2073690

80. Li Y, Song X, Liu L, Yue L. NUAK2 silencing inhibits the proliferation, migration and epithelial-to-mesenchymal transition of cervical cancer cells via upregulating CYFIP2. Mol Med Rep. 2021;24. doi:10.3892/mmr.2021.12457

81. Steffen A, Rottner K, Ehinger J, Innocenti M, Scita G, Wehland J, et al. Sra-1 and Nap1 link Rac to actin assembly driving lamellipodia formation. EMBO J. 2004;23: 749–759. doi:10.1038/sj.emboj.7600084

82. Rubeis SD, Pasciuto E, Li KW, Fernandez E, Marino DD, Buzzi A, et al. CYFIP1 coordinates mRNA translation and cytoskeleton remodeling to ensure proper dendritic spine formation. Neuron. 2013;79: 1169–1182. doi:10.1016/j.neuron.2013.06.039 [doi]

83. Pathania M, Davenport EC, Muir J, Sheehan DF, Lopez-Domenech G, Kittler JT. The autism and schizophrenia associated gene CYFIP1 is critical for the maintenance of dendritic complexity and the stabilization of mature spines. Transl Psychiatry. 2014;4: e374. doi:10.1038/tp.2014.16 [doi]

84. Davenport EC, Szulc BR, Drew J, Taylor J, Morgan T, Higgs NF, et al. Autism and Schizophrenia-Associated CYFIP1 Regulates the Balance of Synaptic Excitation and Inhibition. Cell Rep. 2019;26: 2037-2051.e6. doi:S2211-1247(19)30129-9 [pii]

85. Hanneman E, Trevarrow B, Metcalfe WK, Kimmel CB, Westerfield M. Segmental pattern of development of the hindbrain and spinal cord of the zebrafish embryo. Development. 1988;103: 49–58. doi:10.1242/dev.103.1.49

86. Eaton RC, Farley RD. Development of the mauthner neurons in embryos and larvae of the zebrafish, Brachydanio rerio. Copeia. 1973;1973: 673. doi:10.2307/1443067

87. Kimmel CB, Hatta K, Metcalfe WK. Early axonal contacts during development of an identified dendrite in the brain of the zebrafish. Neuron. 1990;4: 535–545. doi:10.1016/0896-6273(90)90111-r

88. Kimmel CB, Sessions SK, Kimmel RJ. Morphogenesis and synaptogenesis of the zebrafish Mauthner neuron. J Comp Neurol. 1981;198: 101–120. doi:10.1002/cne.901980110

89. Tanimoto M, Ota Y, Horikawa K, Oda Y. Auditory input to CNS is acquired coincidentally with development of inner ear after formation of functional afferent pathway in zebrafish. J Neurosci. 2009;29: 2762–2767. doi:10.1523/JNEUROSCI.5530-08.2009

90. Siomi MC, Siomi H, Sauer WH, Srinivasan S, Nussbaum RL, Dreyfuss G. FXR1, an autosomal homolog of the fragile X mental retardation gene. EMBO J. 1995;14: 2401–2408. doi:10.1002/j.1460-2075.1995.tb07237.x

91. Zhang Y, O'Connor JP, Siomi MC, Srinivasan S, Dutra A, Nussbaum RL, et al. The fragile X mental retardation syndrome protein interacts with novel homologs FXR1 and FXR2. EMBO J. 1995;14: 5358–5366. doi:10.1002/j.1460-2075.1995.tb00220.x

92. Bakker CE, de Diego Otero Y, Bontekoe C, Raghoe P, Luteijn T, Hoogeveen AT, et al. Immunocytochemical and biochemical characterization of FMRP, FXR1P, and FXR2P in the mouse. Exp Cell Res. 2000;258: 162–170. doi:10.1006/excr.2000.4932

93. Agulhon C, Blanchet P, Kobetz A, Marchant D, Faucon N, Sarda P, et al. Expression of FMR1, FXR1, and FXR2 genes in human prenatal tissues. J Neuropathol Exp Neurol. 1999;58: 867–880. doi:10.1097/00005072-199908000-00009

94. Tucker B, Richards R, Lardelli M. Expression of three zebrafish orthologs of human FMR1-related genes and their phylogenetic relationships. Dev Genes Evol. 2004;214: 567–574. doi:10.1007/s00427-004-0438-9

95. Coffee RL Jr, Tessier CR, Woodruff EA 3rd, Broadie K. Fragile X mental retardation protein has a unique, evolutionarily conserved neuronal function not shared with FXR1P or FXR2P. Dis Model Mech. 2010;3: 471–485. doi:10.1242/dmm.004598

96. Boczkowska M, Rebowski G, Kast DJ, Dominguez R. Structural analysis of the transitional state of Arp2/3 complex activation by two actin-bound WCAs. Nat Commun. 2014;5: 3308. doi:10.1038/ncomms4308

97. Lacoste AM, Schoppik D, Robson DN, Haesemeyer M, Portugues R, Li JM, et al. A convergent and essential interneuron pathway for Mauthner-cell-mediated escapes. Curr Biol. 2015;25: 1526–1534. doi:10.1016/j.cub.2015.04.025 [doi]

98. Möhrle D, Wang W, Whitehead SN, Schmid S. GABAB Receptor Agonist R-Baclofen Reverses Altered Auditory Reactivity and Filtering in the Cntnap2 Knock-Out Rat. Front Integr Neurosci. 2021;15. doi:10.3389/fnint.2021.710593

99. Waldmeier PC, Kaupmann K, Urwyler S. Roles of GABAB receptor subtypes in presynaptic auto- and heteroreceptor function regulating GABA and glutamate release. J Neural Transm. 2008;115: 1401–1411. doi:10.1007/s00702-008-0095-7

100. Wu C, Sun D. GABA receptors in brain development, function, and injury. Metab Brain Dis. 2015;30: 367–379. doi:10.1007/s11011-014-9560-1

101. Tureček R, Melichar A, Králíková M, Hrušková B. The role of GABAB receptors in the subcortical pathways of the mammalian auditory system. Front Endocrinol . 2023;14: 1195038. doi:10.3389/fendo.2023.1195038

102. Berry-Kravis E, Hagerman R, Visootsak J, Budimirovic D, Kaufmann WE, Cherubini M, et al. Arbaclofen in fragile X syndrome: results of phase 3 trials. J Neurodev Disord. 2017;9: 3. doi:10.1186/s11689-016-9181-6

103. Veenstra-VanderWeele J, Cook EH, King BH, Zarevics P, Cherubini M, Walton-Bowen K, et al. Arbaclofen in Children and Adolescents with Autism Spectrum Disorder: A Randomized, Controlled, Phase 2 Trial. Neuropsychopharmacology. 2017;42: 1390–1398. doi:10.1038/npp.2016.237

104. Erickson CA, Veenstra-Vanderweele JM, Melmed RD, McCracken JT, Ginsberg LD, Sikich L, et al. STX209 (arbaclofen) for autism spectrum disorders: an 8-week open-label study. J Autism Dev Disord. 2014;44: 958–964. doi:10.1007/s10803-013-1963-z

105. Mattson MP, Gleichmann M, Cheng A. Mitochondria in neuroplasticity and neurological disorders. Neuron. 2008;60: 748–766. doi:10.1016/j.neuron.2008.10.010

106. Smith GM, Gallo G. The role of mitochondria in axon development and regeneration. Dev Neurobiol. 2018;78: 221–237. doi:10.1002/dneu.22546

107. Safer D, Elzinga M, Nachmias VT. Thymosin beta 4 and Fx, an actin-sequestering peptide, are indistinguishable. J Biol Chem. 1991;266: 4029–4032. Available: https://www.ncbi.nlm.nih.gov/pubmed/1999398

108. Yu FX, Lin SC, Morrison-Bogorad M, Atkinson MA, Yin HL. Thymosin beta 10 and thymosin beta 4 are both actin monomer sequestering proteins. J Biol Chem. 1993;268: 502–509. doi:10.1016/s0021-9258(18)54179-x

109. Cheng IH, Lin Y-C, Hwang E, Huang H-T, Chang W-H, Liu Y-L, et al. Collagen VI protects against neuronal apoptosis elicited by ultraviolet irradiation via an Akt/phosphatidylinositol 3-kinase signaling pathway. Neuroscience. 2011;183: 178–188. doi:10.1016/j.neuroscience.2011.03.057

110. Fox MA. Novel roles for collagens in wiring the vertebrate nervous system. Curr Opin Cell Biol. 2008;20: 508–513. doi:10.1016/j.ceb.2008.05.003

Figure Legends

Figure 1. Cyfip2 establishes the acoustic startle threshold through Rac1 and FMRP.

(A) Cyfip2 protein interacting domain diagram of wildtype (top) and mutant (bottom) Cyfip2 proteins. Black arrowheads indicate the positions of induced mutations in Cyfip2, eliminating the Rac1- (C179R) or FMRP/eIF4E (K723E)-binding capacity of Cyfip2. (B) Cyfip2 actin regulatory pathway wherein Cyfip2 (orange) upon stimulation by Rac1-GTP triggers WAVE1 activation, Arp2/3-complex initiation and branched actin nucleation. (C) Cyfip2 translational repression pathway in which Cyfip2, eIF4E (teal), and FMRP (pink) along with the poly-A binding protein (PABP; gray), sequester neurodevelopmentally important mRNAs from being translated. (D) Average startle frequency (%) after 10 trials at 13.6, 25.7, 29.2, 35.5, 39.6 and 53.6 dB for 5 dpf *cyfip2* siblings (+/) and mutant (-/-) larvae heatshocked at 30 hpf for 40 minutes at 38˚C. The average startle frequency curve for cyfip2 siblings (+/; open circles, dashed line), cyfip2 mutants (-/-; closed circles, solid line) and cyfip2 mutants harboring the *Tg(hsp70:cyfip2-EGFP)*+ transgene (-/-; Tg+; closed circles, solid green line). (E) Sensitivity indices, calculated as the area under the startle frequency curves, for 5 dpf cyfip2 siblings and mutants, following a 40-minute heatshock at 30 hpf to express either wildtype (Tg+; green), Rac1- (ΔRac1+; blue) or FMRP/eIF4E- (ΔFMRP+; pink) binding deficient versions of Cyfip2-EGFP. Comparisons were made to both non-transgenic (Tg-) and non-heatshocked controls. All indices (mean ± SD) compared using a Kruskal-Wallis test with Dunn's multiple comparisons correction; p**** < 0.0001. (F) Sensitivity indices for 5 dpf *cyfip2* sibling (+/) and mutant (-/-) larvae following 1-cell stage injection with CRISPR-Cas9 and a single, scrambled guide RNA (gRNA) or dual gRNA cocktails targeting *fmr1*, *fxr1*, or *fxr2*. scrambled gRNA injected (white bar, closed circles); fmr1 gRNA injected (dark gray bar closed circles); *fxr1* gRNA injected (medium gray bar; closed circles); *fxr2* gRNA injected (light gray bar, closed circles). Comparisons were made both within genotype and between genotypes by condition. All indices (mean ± SD) compared using an Ordinary one-way ANOVA with Sidak's multiple comparisons correction; p* < 0.05; p** < 0.01; p**** < 0.0001.

Figure 2. Cyfip2 acutely regulates branched actin polymerization and NMDARs to establish the acoustic startle threshold.

(A) Sensitivity indices for 5 dpf *cyfip2* sibling (+/) and mutant (-/-) larvae, following a 40-minute heatshock at 120 hpf (5 dpf) to express either wildtype (Tg+; green), Rac1- (ΔRac1+; blue) or FMRP/eIF4E- (ΔFMRP+; pink) binding deficient versions of Cyfip2-EGFP. Comparisons were made to non-transgenic (Tg-), heatshocked sibling (+/) and mutant (-/-) controls. All indices (mean ± SD) compared using a Kruskal-Wallis test with Dunn's multiple comparisons correction; p-values listed; p** < 0.01, p**** < 0.0001. (B) Sensitivity indices for 5 dpf *cyfip2* wildtype (+/+; white bar) and heterozygous (+/-; gray bar) larvae, treated for 30 minutes on d5 with 5, 20 or 50 μM CK-869. Comparisons were made both within genotype and within condition. All indices (mean ± SD) compared using a Kruskal-Wallis test with Dunn's multiple comparisons correction; p* < 0.05; p**** < 0.0001. (C) Sensitivity indices for 5 dpf Tüpfel longfin (TL) larvae treated for 30 minutes on d5 with the highest, non-lethal doses the formin antagonist (SMIFH2; 5 μM), PAK3 antagonist (IPA-3; 50 μM) and ROCK antagonist (GSK429286; 100 μM). Comparisons were made between respective treatments and the DMSO controls. All indices (mean ± SD) were compared using a Kruskal-Wallis test with Dunn's multiple comparisons correction; All comparisons made were non-significant (n.s.). (D) Sensitivity indices for 5 dpf *cyfip2* sibling (+/) and mutant (-/-) larvae, treated for 30 minutes on d5 with 100 or 500 μM MK-801. Comparisons were made both between genotypes within condition and between conditions by genotype. All indices (mean ± SD) were compared using an Ordinary one-way ANOVA with Tukey's multiple comparisons correction. p** < 0.01; p*** < 0.001; p**** < 0.0001.

Figure 3. Loss of Cyfip2 causes widespread proteomic changes and GABAB receptor signaling is critical for startle sensitivity.

(A) Bubble plots reporting the level of significance of the top 10 dysregulated proteins for both *cyfip2* heterozygous (top) and mutant (bottom) groups compared to wildtype controls. The size of the dot is proportional to the significance of the results while the color code represents the log2 fold change; top five upregulated (green), and top five downregulated (red) proteins are shown. (B-C) Heat maps displaying the impacted canonical pathways (B) and diseases and biological functions (C) from IPA functional analysis. The blue-colored gradient indicates the degree of enrichment for the listed pathways or diseases/functions, as represented by the – log of the P value for each pathway, disease and/or function. (D-E) Sensitivity indices for 5 dpf *cyfip2* sibling (+/) and mutant (-/-) larvae, treated for 60 minutes prior to testing with muscimol (D) or (E) baclofen. All indices (mean ± SD) were compared using a one-way ANOVA with Sidak's multiple comparisons correction. p* < 0.05, p** < 0.01; p*** < 0.001; p**** < 0.0001.

Tables

Compound	Concentration (μM)	Effect By Genotype		
		cyfip2(+/+)	***cyfip2(+/-)***	***cyfip2(-/-)***
NPAA (Cl- channel antagonist)	1	93.21% of Control, p > 0.99	110.21% of Control, p < 0.99	113.57% of Control, p > 0.99
	5	140.11% of Control, p = 0.9785	137.32% of Control, p = 0.1385	140.29% of Control, p > 0.2787
	10	**234.14% of Control, p** = 0.0038**	**201.29% of Control, p**** < 0.0001**	**155.06% of Control, p* = 0.0189**
MA (K+ channel/gap jxn. antagonist)	1	131.6% of Control, p > 0.99	11.87% of Control, p > 0.99	132.29% of Control, p = 0.5732
	5	137.24% of Control, p > 0.99	138.46% of Control, p = 0.0622	112.29% of Control, p > 0.99
	10	214.13% of Control, p = 0.0833	**169.81% of Control, p* = 0.0188**	**155.76% of Control, p* = 0.0288**
POBA (AAR/calmodulin antagonist)	1	102.9% of Control, p > 0.99	107.08% of Control, p > 0.99	101.04% of Control, p > 0.99
	10	136.17% of Control, p > 0.99	106.58% of Control, p > 0.99	99.01% of Control, p > 0.99

	50	**175.8% of Control, p* = 0.0123**		99.76% of Control, p > 0.99
ETAZ (PDE4 inhibitor)	1	141.79% of Control, p > 0.99	126.36% of Control, p > 0.99	121.74% of Control, p > 0.99
	10	168.6% of Control, p = 0.5472	**172.26% of Control, p* = 0.0137**	152.73% of Control, p = 0.3977
	50	**236.64% of Control, p** = 0.0029**	**179.99% of Control, p** = 0.0015**	**149.75% of Control, p* = 0.0105**
MK-801 (NMDAR antagonist)	100	120.19% of Control, p > 0.99		**145.93% of Control, p** = 0.0024**
	500	**212.69% of Control, p**** < 0.0001**		**163.26% of Control, p*** = 0.0002**
BMS-204352 (K+ channel antagonist)	10	79.48% of Control, p = 0.4269		89.55% of Control, p > 0.99
	50	76.08% of Control, p = 0.6759		108.74% of Control, p > 0.99
NSC-23766 (Rac1 antagonist)	100	**49.14% of Control, p*** = 0.0002**		81.60% of Control, p > 0.99
	200	86.26% of Control, p > 0.99		105.28% of Control, p > 0.99

Table 1. Cyfip2 may regulate NMDARs to control acoustic startle sensitivity. Mean startle index comparisons, listed as percentage (%) of the mean startle index of vehicle-treated controls by *cyfip2* genotype and drug concentration, for larvae treated with compounds targeting the indicated pathways [59] to increase acoustic startle sensitivity. All significant differences ($p < 0.05$) are listed (**bold**) for comparisons using a Kruskal-Wallis test and Dunn's multiple comparisons correction. NPAA (*N*-phenylanthranilic acid); MA (meclofenamic acid); POBA (phenoxybenzamine); ETAZ (etazolate).

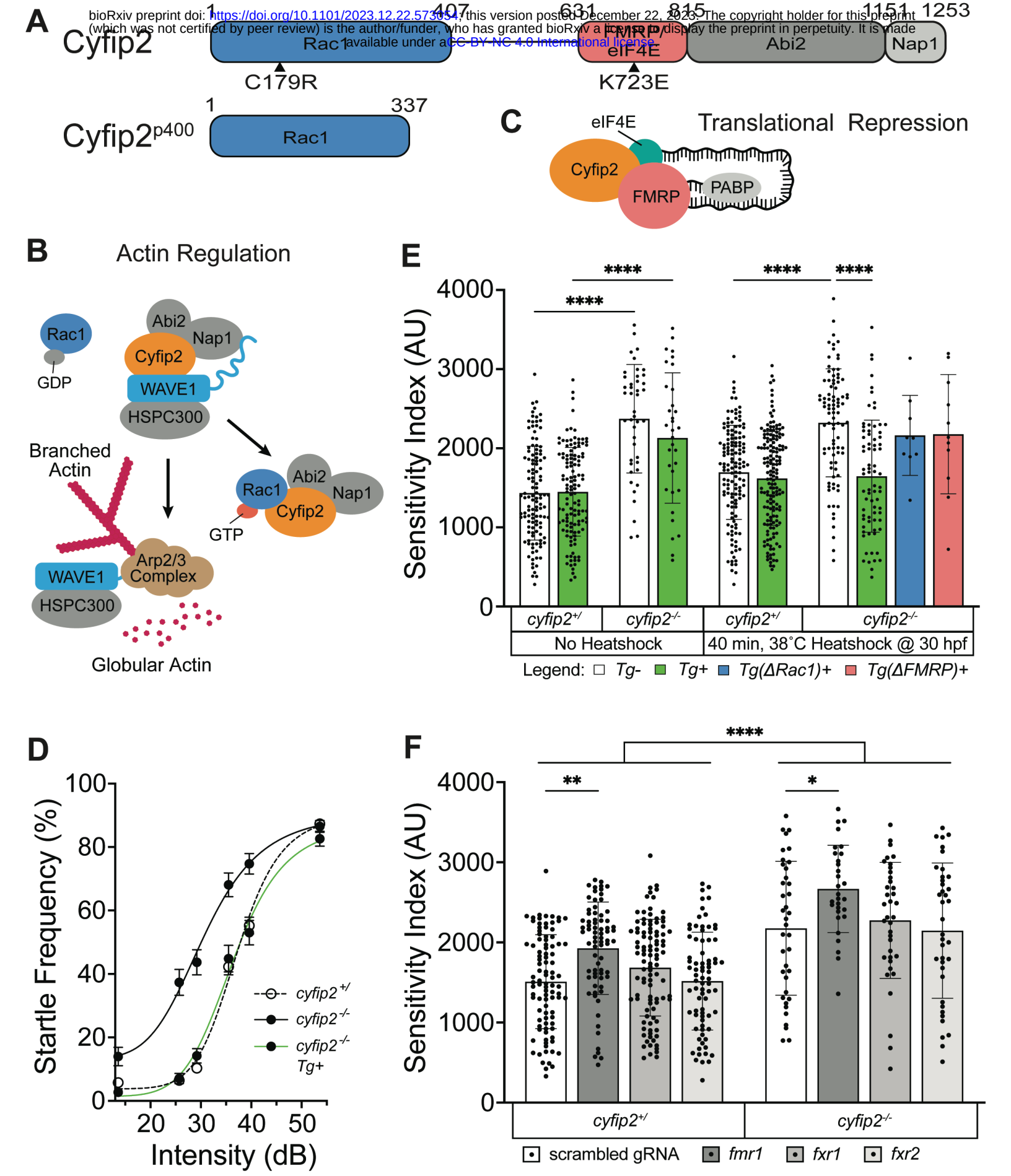

Figure 1 Deslauriers et al. 2023

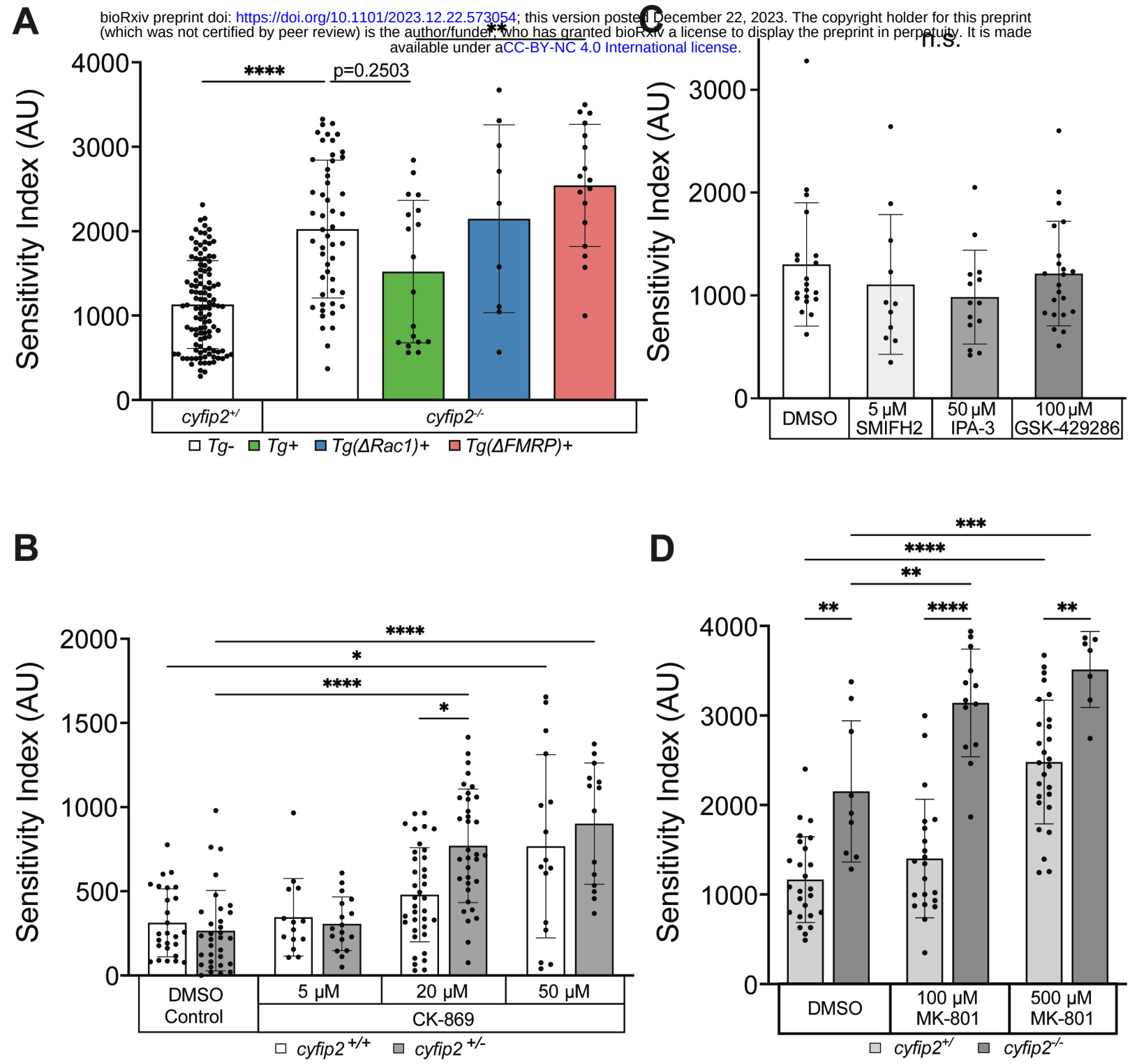

Figure 2 Deslauriers et al. 2023

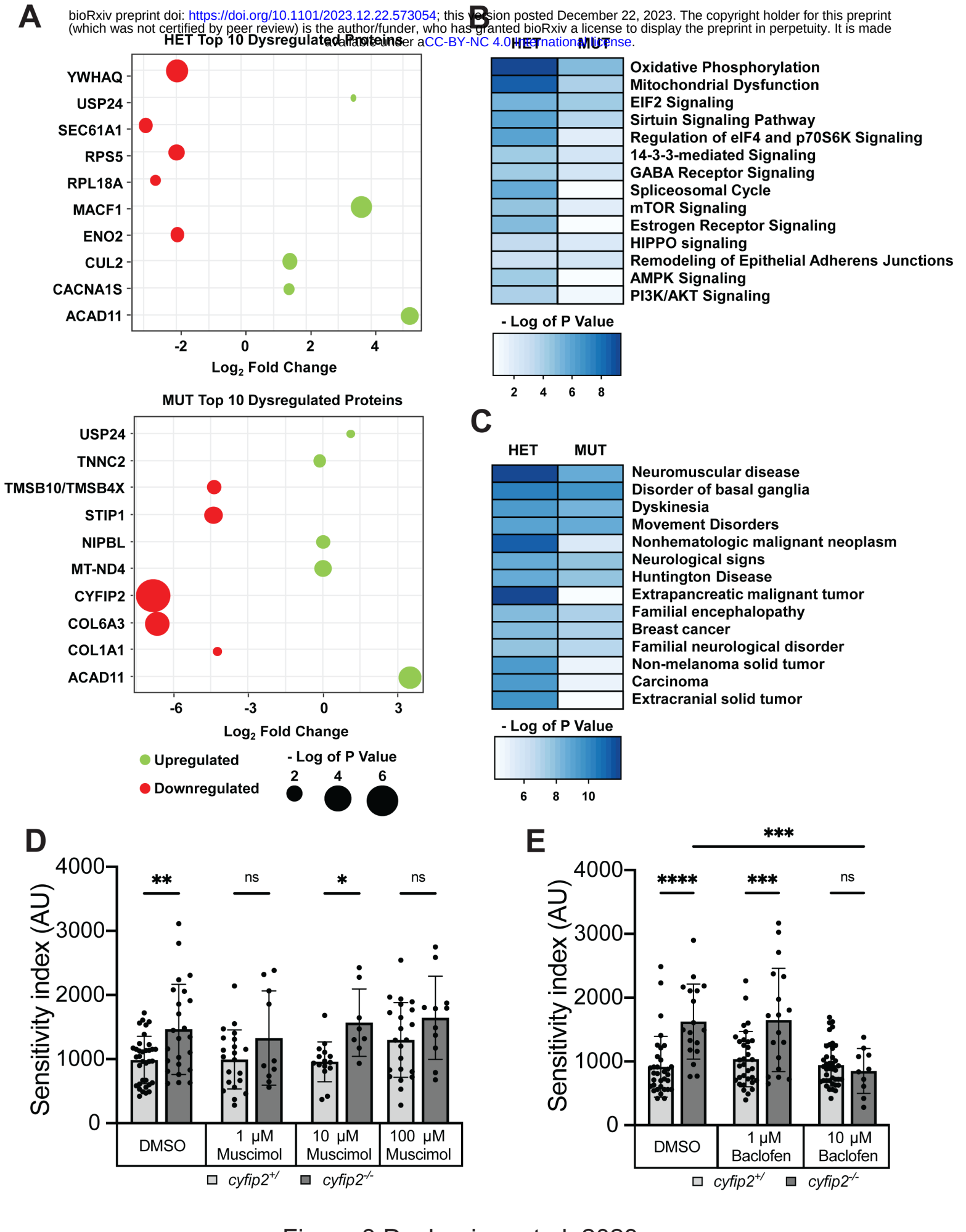

Figure 3 Deslauriers et al. 2023